

A rigorous hybridization of variational quantum eigensolver and classical neural network

Minwoo Kim,^{1, 2, 3} Kyoung Keun Park,^{1, 2, 3} Kyungmin Lee,^{1, 2, 3} Jeongho Bang,^{4, 5, *} and Taehyun Kim^{1, 2, 3, 6, 7, †}

¹Dept. of Computer Science and Engineering, Seoul National University, Seoul 08826, South Korea

²NextQuantum, Seoul National University, Seoul 08826, South Korea

³Automation and Systems Research Institute, Seoul National University, Seoul 08826, South Korea

⁴Institute for Convergence Research and Education in Advanced Technology,

Yonsei University, Seoul 03722, Republic of Korea

⁵Department of Quantum Information, Yonsei University, Incheon 21983, South Korea

⁶Institute of Computer Technology, Seoul National University, Seoul 08826, South Korea

⁷Institute of Applied Physics, Seoul National University, Seoul 08826, South Korea

(Dated: February 20, 2026)

Neural post-processing has been proposed as a lightweight route to enhance variational quantum eigensolvers by learning how to reweight measurement outcomes. In this work, we identify three general desiderata for such data-driven neural post-processing—(i) self-contained training without prior knowledge, (ii) polynomial resources, and (iii) variational consistency—and show that current approaches, such as diagonal non-unitary post-processing (DNP), cannot satisfy these requirements simultaneously. The obstruction is intrinsic: with finite sampling, normalization becomes a statistical bottleneck, and support mismatch between numerator and denominator estimators can render the empirical objective ill-conditioned and even sub-variational. Moreover, to reproduce the ground state with constant-depth ansatzes or with linear-depth circuits forming unitary 2-designs, the required reweighting range (and hence the sampling cost) grows exponentially with the number of qubits. Motivated by this no-go result, we develop a normalization-free alternative, the unitary variational quantum-neural hybrid eigensolver (U-VQNHE). U-VQNHE retains the practical appeal of a learnable diagonal post-processing layer while guaranteeing variational safety, and numerical experiments on transverse-field Ising models demonstrate improved accuracy and robustness over both VQE and DNP-based variants.

I. INTRODUCTION

Variational quantum eigensolver (VQE) [1, 2] is a paradigmatic near-term algorithm for estimating ground-state energies in chemistry and condensed-matter physics [3–5]. Its appeal is not only practical—a shallow parametrized quantum circuit (PQC) executed on noisy intermediate-scale quantum (NISQ) hardware [6]—but also physical. Namely, for any normalized trial state, the Rayleigh–Ritz variational principle guarantees that the measured energy is an upper bound on the true ground-state energy [7]. This bound provides a built-in “sanity check” throughout optimization: values that undershoot the ground state are not merely inaccurate, but indicate that the procedure has departed from a legitimate quantum-state evaluation.

As variational quantum algorithms (VQAs) matured into a broad framework for optimization and quantum machine learning [8, 9], it became natural to hybridize with classical learning systems. One line of work replaces parts of classical architectures with PQCs to exploit quantum representations [10–13]. A complementary line places the neural networks as a post-processing (or pre-processing) module around a variational circuit. Here, the neural encoders can learn problem-adapted

embeddings and warm-starts [14–18], while the learned post-processing can mitigate readout bias, denoise observables, and reweight samples [19–21]. These hybrids promise extra flexibility at modest overhead, but they also raise a critical question to be considered seriously: which structural features of the variational loop must be preserved for the results to remain physically meaningful?

In this work, we study a broad and practically relevant class of neural post-processing layers that act diagonally on measurement outcomes. Operationally, a neural network reads each measured bit string (or, more generally, each measurement record $x \in \Omega$) and outputs a nonnegative weight; expectation values are then evaluated after reweighting the shot data and renormalizing. Because the action is diagonal, the additional classical overhead can remain polynomial, making such schemes attractive as “plug-in” upgrades to existing VQE pipelines. This diagonal reweighting philosophy appears in several recent proposals; throughout the paper we refer to the resulting abstraction as diagonal non-unitary post-processing (DNP).

The subtlety is that DNP necessarily turns the energy evaluation into a normalized ratio estimator. In realistic shot-based implementations, the numerator and denominator of the ratio are estimated from distinct measurement ensembles, so finite-sampling errors can enter asymmetrically through the normalization. This asymmetry is precisely where variational safety can be lost:

* jbang@yonsei.ac.kr

† taehyun@snu.ac.kr

the optimizer may exploit statistical ‘‘loopholes’’ of the empirical normalization and drive the estimated energy below the Rayleigh–Ritz bound, even though the underlying goal remains ground state preparation. This motivates the central question: Can a data-driven neural post-processing layer be simultaneously (i) self-contained (no prior knowledge of the ground state), (ii) scalable with polynomial quantum and classical resources, and (iii) variationally consistent under finite sampling?

Our main result answers this question in the negative for DNP. We show that the non-unitary nature of diagonal reweighting makes normalization a statistical bottleneck: unless one expends exponentially many measurements, the empirical DNP objective can become ill-conditioned and may yield sub-variational (hence non-physical) energies. We further prove that even if one stabilizes training by constraining the output range of the neural network, reproducing the ground state generically demands an exponentially large reweighting range for both (i) constant-depth ansatz circuits and (ii) linear-depth ansatz circuits in the unitary 2-design regime. Together, these results establish a rigorous resource-consistency obstruction for DNP-type hybridization.

Motivated by this obstruction, we introduce a normalization-free design principle by enforcing norm preservation by construction. More concretely, we propose the unitary variational quantum-neural hybrid eigensolver (U-VQNHE), which replaces non-unitary diagonal reweighting with a learnable diagonal unitary post-processing layer (a phase-only transformation). Because the post-processing is unitary, the object whose energy is evaluated remains a normalized quantum state, and the Rayleigh–Ritz bound is preserved by construction. U-VQNHE thus retains the practical appeal of a learnable diagonal post-processing module—with at most a constant-factor measurement overhead—while eliminating the normalization-induced failure mode of DNP.

Our contributions can be summarized as follows:

- We formulate a unified abstraction for diagonal neural post-processing and identify three desiderata (self-contained training, polynomial resources, and variational consistency) that any such protocol should satisfy.
- We prove that DNP(-type) cannot satisfy these desiderata simultaneously: finite-shot normalization induces an intrinsic instability, and accurate ground-state reconstruction requires an exponentially growing reweighting range (hence exponential sampling) for both trainable constant-depth ansatzes and linear-depth 2-design circuits.
- We propose U-VQNHE, a diagonal unitary post-processing scheme that removes explicit normalization, guarantees variational safety, and improves robustness and accuracy on transverse-field Ising models.

II. DIAGONAL NON-UNITARY POST-PROCESSING ON VQE

In the VQE framework, a parameterized unitary $U(\boldsymbol{\theta})$ prepares a variational state

$$|\psi(\boldsymbol{\theta})\rangle = U(\boldsymbol{\theta})|0\rangle^{\otimes n}, \quad (1)$$

which yields the energy expectation value $E(\boldsymbol{\theta}) = \langle\psi(\boldsymbol{\theta})|H|\psi(\boldsymbol{\theta})\rangle$, minimized with respect to $\boldsymbol{\theta}$. Here the Hamiltonian is expressed as a weighted sum of Pauli strings, $H = \sum_P c_P P$, whose expectation values are measurable directly from the quantum circuits via basis transformation [1, 22]. This setup guarantees, from the Rayleigh-Ritz variational principle, that for any circuit ansatz it holds that

$$\min_{\boldsymbol{\theta}} E(\boldsymbol{\theta}) \geq E_{\text{gs}}, \quad (2)$$

where E_{gs} is the ground state energy of the system. Thus, the goal of VQE is to find the set of parameters $\boldsymbol{\theta}$ that minimizes the expectation value of the Hamiltonian via a classical optimizer.

A. Diagonal non-unitary post-processing

DNP extends this paradigm by introducing a classical post-processing procedure that reshapes the measurement distribution generated by the circuit. Instead of directly evaluating the expectation value of the Hamiltonian on $|\psi(\boldsymbol{\theta})\rangle$, it applies a diagonal reweighting operation represented by a generally non-unitary map

$$\mathcal{D}_f(\rho) = \frac{D_f \rho D_f^\dagger}{\text{Tr}[D_f \rho D_f^\dagger]}, \quad D_f = \sum_{x \in \Omega} f(x) |x\rangle\langle x|, \quad (3)$$

where $f(x) \in \mathbb{R}$ (or \mathbb{C}) is a parametrized neural network, acting as a function of the measurement output x . Here, Ω denotes the domain of measurement records used in post-processing: in the standard setting $\Omega = \{0, 1\}^n$ and $x = s$ is the computational-basis bit string of the system qubits, whereas in some algorithmic variants Ω may be extended to include additional measured bits or exclude certain bits. Although it can be generalized to encompass complex numbers, we discuss real-valued neural networks in what follows for simplicity.

The transformation acts as a nonlinear channel on the density operator and, for a pure input state $\rho = |\psi(\boldsymbol{\theta})\rangle\langle\psi(\boldsymbol{\theta})|$, produces the normalized, post-processed state

$$|\tilde{\psi}(\boldsymbol{\theta})\rangle_f = \frac{D_f |\psi(\boldsymbol{\theta})\rangle}{\|D_f |\psi(\boldsymbol{\theta})\rangle\|}, \quad (4)$$

where $\|D_f |\psi(\boldsymbol{\theta})\rangle\| = \sqrt{\langle\psi(\boldsymbol{\theta})|D_f^\dagger D_f |\psi(\boldsymbol{\theta})\rangle}$ ensures proper normalization. The corresponding variational energy functional becomes

$$E_f(\boldsymbol{\theta}) = \frac{\langle\psi(\boldsymbol{\theta})|D_f^\dagger H D_f |\psi(\boldsymbol{\theta})\rangle}{\langle\psi(\boldsymbol{\theta})|D_f^\dagger D_f |\psi(\boldsymbol{\theta})\rangle}. \quad (5)$$

The neural network takes this energy functional as its loss function and repeatedly optimizes the parameters to minimize the loss.

This expression generalizes the standard VQE energy functional, in which the observable expectation value is a linear functional of the prepared quantum state. The diagonal map D_f redefines the variational objective as a nonlinear ratio of reweighted expectation values, effectively acting as a data-dependent filter on the probability amplitudes of $|\psi(\theta)\rangle$ in the computational basis. It modifies the underlying Born distribution for each Pauli term in the computational basis, while preserving normalization through the denominator in Eq. (5). This construction recovers VQNHE [23], which uses a single classical neural network $f(s) : \{0, 1\}^n \rightarrow \mathbb{R}$ or \mathbb{C} , trained on top of the quantum circuit to minimize $E_f(\theta)$. Joint training of the quantum and neural parameters is possible, but only when sufficient accuracy is guaranteed by the quantum-circuit measurements. We discuss this in Appendix F. Expanding the choice of measurement record $x \in \Omega$ and the corresponding estimators yields a broader representation encompassing some algorithmic variants (Appendix B), all sharing the same diagonal non-unitary structure.

Consequently, Eq. (5) can be regarded as a general variational formulation in which the energy functional depends not only on the unitary circuit parameters θ but also on the classical parameters defining a nonlinear transformation of the sampling distribution. This abstraction places the aforementioned algorithms within a unified theoretical framework and clarifies that such methods correspond to optimizing an expectation value with respect to a post-processed quantum state $|\tilde{\psi}(\theta)\rangle_f$ defined by a diagonal non-unitary map. This formulation highlights the broader applicability of parametrized quantum circuits when combined with diagonal channels of the form (3), which may improve representational accuracy and convergence efficiency of hybrid quantum-classical algorithms at the cost of modified normalization and sampling complexity, as analyzed in the following sections.

B. General expectation-value evaluation via circuit transformations

Following Ref. [23], the neural network training objective in Eq. (5) reduces to estimating normalized contributions of the form

$$\frac{\langle \psi(\theta) | D_f^\dagger P D_f | \psi(\theta) \rangle}{\langle \psi(\theta) | D_f^\dagger D_f | \psi(\theta) \rangle} \quad \text{for each Pauli string } P. \quad (6)$$

The expectation value entering the diagonal post-processing functional can be evaluated using a circuit-transformation scheme. The basic idea follows the original formulation of VQNHE [23]: for each Pauli term of the Hamiltonian, the measurement basis is rotated so

that the corresponding operator is effectively diagonalized, and the resulting bit strings are reweighted by the diagonal function f during classical post-processing.

Concretely, for each Pauli term P , a short, fixed-depth transformation is applied to align the measurement basis with the eigenbasis of P . This involves adding a local entangling operation that coherently encodes the relevant Pauli parity onto a single reference qubit, followed by appropriate single-qubit rotations (H or $R_X(\pi/2)$) that map all Pauli factors to the Z basis. After this step, the circuit is measured in the computational basis, yielding an outcome record $x \in \Omega$ (typically $x = s \in \{0, 1\}^n$). Conceptually, this converts the action of the operator P into a pairwise-diagonal form, where each observed bit string s is naturally associated with its partner \tilde{s}_P obtained by flipping the bits corresponding to the non- Z components of P . This allows for efficient evaluation of the energy estimator. Refer to Appendix A for details and notations used.

C. Criteria for Stable and Variationally Safe Training

Before quantifying resource requirements, we make explicit which properties a neural post-processing module must preserve in order to be a meaningful extension of a variational quantum algorithm. The following desiderata formalize what it means for a post-processing layer to be “scalable” and “physically interpretable,” and they also clarify precisely where DNP fails under finite sampling.

Definition 1 (Desiderata for data-driven neural post-processing). *We say that a neural post-processing protocol is stable and variationally safe if it satisfies all of the following:*

- 1. Self-contained training (no prior knowledge).** *The neural network is trained solely from measurement outcomes on the quantum device during the variational loop, without access to the exact ground state, its energy, or large precomputed training sets.*
- 2. Polynomial resource scaling.** *The number of distinct quantum circuits, the number of shots per circuit, and the classical overhead (including neural-network size and training cost) scale at most polynomially with the number of qubits n .*
- 3. Variational consistency.** *The reported energy values remain consistent with the Rayleigh–Ritz principle: in the ideal noiseless limit, the objective corresponds to the expectation value of H on a normalized quantum state, and therefore cannot undershoot the true ground-state energy E_{gs} .*

Remark 1 (Why variational consistency becomes non-trivial for DNP). *For any exactly normalized post-processed state $|\psi\rangle$ (including the formal DNP state in*

Eq. (4)), the variational bound $\langle \psi | H | \psi \rangle \geq E_{\text{gs}}$ holds automatically. The subtlety is that practical DNP implementations do not evaluate Eq. (5) exactly: they estimate its numerator and denominator from independent finite-shot ensembles and optimize the resulting empirical ratio \hat{E}_f . This empirical ratio need not coincide with the expectation value of any normalized quantum state and can therefore violate the variational bound unless one expends exponentially many samples.

The DNP schemes are, at first sight, compatible with the first two desiderata: the network can be trained on-device without supervision, and the diagonal structure keeps the additional classical overhead polynomial. Our central message is that the third desideratum is the bottleneck: in DNP, the normalization itself becomes a sampling-limited quantity. The rest of the paper makes this statement quantitative by analyzing (i) when the empirical normalization can fail catastrophically and (ii) how stabilizing constraints on the neural network introduce an unavoidable tradeoff between expressiveness and sampling cost.

III. EXPONENTIAL RESOURCE REQUIREMENT FOR DNP

As established in Eq. (5), DNP transforms the standard variational objective into a normalized ratio, $E_f(\boldsymbol{\theta}) = \sum_P c_P \frac{N_f(P)}{Z_f}$, where

$$N_f(P) = \langle \psi(\boldsymbol{\theta}) | D_f^\dagger P D_f | \psi(\boldsymbol{\theta}) \rangle, \quad (7)$$

$$Z_f = \langle \psi(\boldsymbol{\theta}) | D_f^\dagger D_f | \psi(\boldsymbol{\theta}) \rangle = \mathbb{E}_{s \sim p_\psi} [|f(s)|^2].$$

Both energy evaluation and gradient estimation therefore hinge on accurately estimating the normalization Z_f . When D_f is non-unitary, the associated weights $w(s) = |f(s)|^2$ distort the underlying Born distribution $p_\psi(s)$, often concentrating it on a few rare outcomes as training proceeds. This can induce statistical instabilities in normalized observables and cause divergence during neural-network training. In the following, we show that preventing such divergence requires exponentially many measurements.

A. Shot-based formulation

In the following sections, we discuss the DNP formulation in the context of VQNHE [23] as a representative example. In shot-based implementations, the numerator and denominator of Eq. (5) are obtained from distinct measurement ensembles. The denominator,

$$Z_f = \mathbb{E}_{s \sim p_\psi} [|f(s)|^2], \quad (8)$$

is evaluated by sampling the ansatz circuit $U(\boldsymbol{\theta})$ directly in the computational basis, while the numerator requires

additional measurement circuits. For a given Pauli string P , the corresponding expectation value is estimated from outcomes $\{s_i\} \sim p_P$ (the distribution induced by the measurement-augmented circuit for term P). Accordingly, we write the probability distribution of the ansatz p_ψ as p_I .

With M_P measurements for each Pauli term and M_I measurements for the ansatz, the finite-shot estimators are

$$\begin{aligned} \hat{N}_f(P) &= \frac{1}{M_P} \sum_{i=1}^{M_P} \sigma_P(s_i) f(s'_i) f(\tilde{s}'_{i,P}), \\ \hat{Z}_f &= \frac{1}{M_I} \sum_{i=1}^{M_I} f(s_i)^2, \end{aligned} \quad (9)$$

where s_i denotes the sampled bit string. Here, s'_i is obtained by setting the star-qubit bit s_{i*} to zero, and $\tilde{s}'_{i,P}$ is the paired bit string defined by the Pauli-induced mapping for term P (see Appendix A for details). The sign factor $\sigma_P(s_i) = (-1)^{s_{i*}}$ encodes the parity of the star-qubit outcome s_{i*} and corresponds to the measured eigenvalue ± 1 of P . In this measurement setting, the general parity rule reduces to this single-bit sign.

B. Divergence of unconstrained DNP under sub-exponential number of measurements

The stability of the DNP estimator depends crucially on two factors: (i) the degree of overlap between the sampling supports of the numerator and denominator in Eq. (9), and (ii) the constraints imposed on the neural network that defines the weights. In this section, we show that if no explicit regularization or range constraint is applied to the neural-network outputs—beyond the definitional requirement that $f(s) \geq 0$ for all s , since each $f(s)$ acts as a nonnegative weight on a probability component—then exponentially many measurements are required to guarantee arbitrary accuracy. Under any sub-exponential measurement budget, the estimator is generally vulnerable to divergent behavior, often driving the neural network toward large negative values.

To address these issues, we introduce notation for the sampled supports of the numerator and denominator. Let B_a denote the set of bit strings actually observed from the ansatz circuit, and let $B_{m,P}$ denote the set of bit strings observed from the measurement circuit associated with term P . The total set of configurations that can contribute to the numerator is

$$B_M = \bigcup_P \{s', \tilde{s}'_P : s' \in B_{m,P}\}, \quad (10)$$

where \tilde{s}'_P denotes the partner configuration paired with s' by the Pauli term P . For the empirical ratio estimator to be stably normalized, it is necessary that every configuration appearing in the numerator is also sampled; that

is,

$$B_M \subseteq B_a. \quad (11)$$

Proposition 1 (Support mismatch yields an unbounded empirical objective). *Fix a finite-shot dataset used to evaluate the estimators in Eq. (9), and let B_a and B_M denote the sampled supports of the denominator and numerator, respectively. If the support-inclusion condition (11) is violated, i.e., $B_M \not\subseteq B_a$, then the empirical DNP objective $\hat{E}_f = \sum_P c_P \hat{N}_f(P) / \hat{Z}_f$ is, in general, not bounded from below over nonnegative weight functions f . More precisely, whenever there exists a configuration $s_* \in B_M \setminus B_a$ that appears in at least one numerator contribution with a negative effective coefficient, one can choose a sequence of nonnegative functions $\{f_k\}_{k \geq 1}$ such that $\hat{E}_{f_k} \rightarrow -\infty$ while \hat{Z}_{f_k} remains unchanged.*

Proof. —By assumption, there exists a term P_* and a sample outcome in the P_* -measurement ensemble B_{m, P_*} for which either $s' = s_*$ or $\tilde{s}' P_* = s_*$ appears in the numerator with an overall negative prefactor. Freeze all neural outputs except at s_* , and define $f_k(s_*) = k$ with $k \rightarrow \infty$. Because $s_* \notin B_a$, the denominator estimator \hat{Z}_f (an empirical average over B_a) is independent of k . In contrast, the numerator estimator for P_* contains a contribution proportional to k with negative sign, so $\hat{N}_{f_k}(P_*)$ decreases without bound as $k \rightarrow \infty$, and therefore so does \hat{E}_{f_k} . \square

Proposition 1 shows that, under finite sampling, the DNP loss landscape can acquire directions in which the empirical objective decreases without any normalization penalty. This is a structural instability of the ratio estimator: it disappears only when the denominator samples all configurations that can influence the numerator, i.e., when (11) holds. If this subset condition is violated, some configurations appear only in the numerator and never in the denominator, so their contributions are not properly balanced in the normalized ratio $\hat{E}_f = \sum_P c_P \hat{N}_f(P) / \hat{Z}_f$.

To see the consequences more explicitly, consider a configuration $s^* \in B_M \setminus B_a$ that arises in the numerator but is never observed in the ansatz samples. Because the denominator \hat{Z}_f is computed only over B_a , there is no term $|f(s^*)|^2$ to counterbalance the corresponding numerator contribution $c_P f(s^*) f(\tilde{s}_P^*) \sigma_P(s^*)$. As a result, this contribution can grow arbitrarily large in magnitude without being compensated by the normalization. During neural-network training, this imbalance can induce a feedback loop: the loss gradient encourages the mismatching terms to increase whenever doing so lowers the estimated energy, whereas the denominator remains insensitive to this change as long as s^* is not sampled. Consequently, $f(s)$ can be driven toward extreme values on such unseen configurations, pushing \hat{E}_f toward divergence even though all $f(s)$ remain nonnegative and numerically finite.

To quantify how costly it is to avoid this scenario, let $N_M = |B_M|$ denote the number of distinct numerator

configurations, which can be as large as 2^n . Determining the exact number of ansatz shots required to guarantee the support-inclusion event $B_M \subseteq B_a$ is nontrivial in general, because B_M itself depends on the measurement circuits and the finite-shot data. Nevertheless, the scaling is already visible in the most favorable case where the ansatz distribution is uniform over all 2^n computational-basis strings. Conditioned on a fixed set B_M with $N_M = |B_M|$, collecting all configurations in B_M by repeated i.i.d. uniform sampling is precisely a coupon-collector problem [24]. In this setting, the expected number of ansatz shots required to observe every configuration in B_M at least once is

$$\mathbb{E}[M_I] = 2^n H_{N_M}, \quad (12)$$

where $H_{N_M} = \sum_{i=1}^{N_M} \frac{1}{i} = \Theta(\log N_M)$ is the N_M -th harmonic number.

Proposition 2 (Coupon-collector scaling for support inclusion). *Assume that ansatz measurements are i.i.d. and uniform on $\{0, 1\}^n$, and condition on a fixed numerator support set $B_M \subseteq \{0, 1\}^n$ with $N_M = |B_M|$. Let M_I denote the (random) number of ansatz shots required until every configuration in B_M has appeared at least once in the ansatz samples (equivalently, until $B_M \subseteq B_a$ holds). Then, $\mathbb{E}[M_I] = 2^n H_{N_M}$ as in Eq. (12). Moreover, for any $\delta \in (0, 1)$, if $M_I^{(\delta)} \geq 2^n \log(N_M/\delta)$ ansatz shots are taken, then the support inclusion event holds with probability at least $1 - \delta$. In particular, if N_M grows exponentially with n , then enforcing $B_M \subseteq B_a$ with non-negligible success probability requires exponentially many ansatz measurements.*

Proof. —For the expectation, reveal the desired configurations one by one. After k distinct elements of B_M have been observed, the probability that the next uniform ansatz shot produces a new element of B_M is $(N_M - k)/2^n$. Hence, the expected waiting time to increase the number of collected elements from k to $k+1$ is $2^n/(N_M - k)$. Summing over $k = 0, 1, \dots, N_M - 1$ gives

$$\mathbb{E}[M_I] = \sum_{k=0}^{N_M-1} \frac{2^n}{N_M - k} = 2^n \sum_{j=1}^{N_M} \frac{1}{j} = 2^n H_{N_M}. \quad (13)$$

For the high-probability bound, fix any $s \in B_M$. The probability that s is never observed in M uniform shots is $(1 - 2^{-n})^M \leq \exp(-M/2^n)$. By the union bound over the N_M configurations in B_M ,

$$\Pr(B_M \not\subseteq B_a) \leq N_M \exp(-M/2^n). \quad (14)$$

Choosing $M = M_I^{(\delta)} \geq 2^n \log(N_M/\delta)$ makes the right-hand side at most δ , proving $\Pr(B_M \subseteq B_a) \geq 1 - \delta$. \square

Therefore, under any sub-exponential ansatz-shot budget, one should expect B_a to miss some configurations that can contribute to the numerator, so the condition (11) typically fails. Combined with Proposition 1,

this explains why the empirical DNP objective can acquire spurious “downhill” directions in the polynomial-shot regime, which the neural network may exploit during training.

This effect can be viewed as a fundamental resource-stability tradeoff: a non-unitary map D_f effectively reweights the Born distribution, but each additional degree of freedom in $f(s)$ introduces a potential instability unless the corresponding region of the outcome space is sufficiently sampled. In the limit where M_I scales exponentially, every $s \in B_M$ is represented, and the estimator converges to its well-defined normalized limit. In contrast, with polynomial scale of measurements, the overlap $B_M \cap B_a$ remains partial, the effective normalization denominator \widehat{Z}_f underestimates the true norm, and the post-processed energy collapses toward $-\infty$.

We demonstrate this phenomenon using a VQNHE implementation of a 7-qubit transverse-field Ising model (TFIM), shown in Fig. 1. Figure 1(a) displays the optimization trajectory under a shot-based sampler with 500 measurements per circuit. The estimated energy quickly falls below the exact ground-state value (obtained via exact diagonalization) and diverges to nonphysical magnitudes as the neural network amplifies unsupported configurations. Figure 1(b) visualizes the trained neural function $f(s)$: outputs corresponding to unmeasured bit strings (red) reach extreme values, while those associated with measured configurations (blue) remain bounded. This confirms that the divergence originates from the incomplete overlap between B_M and B_a .

C. Exponential resource requirement of constrained DNP: constant-depth circuits

To mitigate such divergence while maintaining a practical measurement budget, a straightforward strategy is to impose explicit constraints on the output range of the neural network. Such constraints have been introduced, either implicitly or explicitly, to address training instabilities [23, 25]. In earlier formulations, the network outputs were restricted to be strictly positive, i.e., $f(s) > 0$ for all s . Extending this idea, one can bound the outputs within a finite interval $[1/r, r]$ (with $r > 1$), since it is their relative ratios—rather than their absolute magnitudes—that influence the post-processing [23].

Once the neural-network outputs are confined to a bounded interval, the divergence discussed above can be effectively suppressed by choosing a sufficiently small value of r , which limits the worst-case amplification of the estimator. Moreover, Zhang *et al.* derived a condition on the number of measurements required for stable estimation under this constraint, for a desired error tolerance ϵ [23]:

$$N \geq \frac{9r^4}{4} \frac{1}{\epsilon^2}. \quad (15)$$

This condition is presented as an upper bound on the esti-

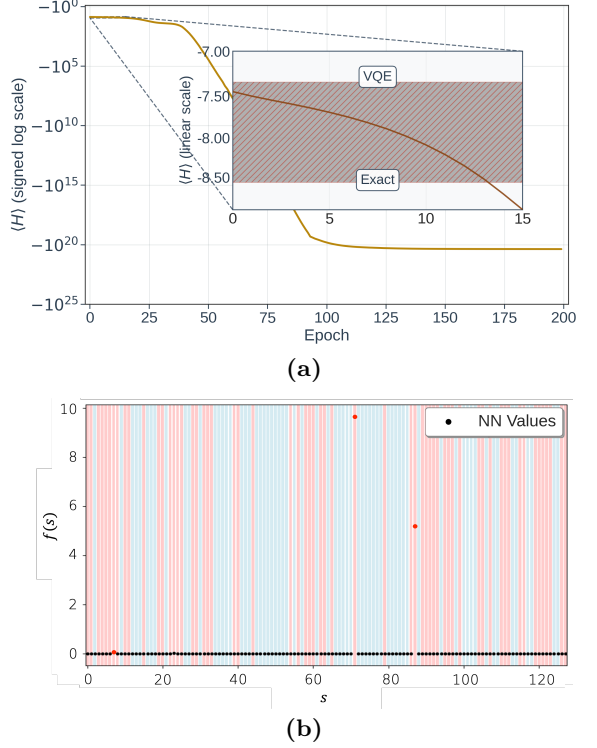


FIG. 1: VQNHE implementation for a 7-site TFIM using 7 qubits. (a) Training dynamics of the neural network within VQNHE. The vertical axis shows the loss function—the expectation value of the Hamiltonian—plotted on a logarithmic scale. Quantum circuit evaluations are performed using the Qiskit sampler with 500 shots per circuit. The inset highlights the region between the lowest vanilla VQE energy and the exact ground state energy, noting that values below this range are nonphysical. (b) Final neural-network outputs after 200 training epochs. The horizontal axis indexes bit strings (in decimal), while the vertical axis shows the corresponding network outputs. Blue lines denote measured bit strings, and red lines denote unmeasured ones. Most outputs cluster near 10^{-6} , whereas a few extreme values (above 10^{-2} ; red) emerge. Since nearly all bit strings are sampled by the quantum circuits, these red points correspond to strings that contribute only to the numerator.

mation error for a fixed number of shots N . Equivalently, it can be interpreted as a lower bound on the required measurement budget: to guarantee that the statistical error does not exceed ϵ , one must allocate at least N measurements satisfying Eq. (15). This reinterpretation emphasizes the operational cost induced by restricting the neural-network outputs and highlights the dependence on the range parameter r . Under this constraint, when both r and N scale polynomially with system size, the DNP estimator yields stable, saturating energy estimates without divergence.

However, avoiding worst-case instability or attaining a small statistical error does not ensure that DNP ac-

curately reproduces the true ground state. If r is chosen too small or the number of measurements N falls short of the convergence criterion in Eq. (15), the post-processed state may still deviate considerably from the exact ground state (and hence its energy). Furthermore, we prove that achieving arbitrarily precise agreement with the true ground state using a constant-depth ansatz combined with DNP reweighting requires the bound parameter r to grow exponentially with the number of qubits. Consequently, both the dynamic range of the neural-network outputs and the number of circuit measurements must increase exponentially in order to represent the ground state accurately, reflecting the resource cost of attaining exact accuracy within the general DNP framework. Without prior knowledge of the ground-state energy, this is not a technical issue but rather a fundamental, architectural caveat arising from the use of non-unitary transformations.

Here, we briefly state the theorem and provide the sketch of its proof, and the remainder is discussed in detail in Appendix C. To show that the neural network requires exponential range to actually reconstruct the ground state from a *finite-depth* ansatz, we compare the fidelity between the ansatz and the ground state in the computational basis. Although this does not represent the actual process of obtaining the expectation values, it is sufficient to show costly requirement of r .

Let $p(s) = |\langle s|\phi_0\rangle|^2$ and $q(s) = |\langle s|\psi_\theta\rangle|^2$ denote the measurement distributions of the ground state and the variational ansatz, respectively. By definition of the diagonal map D_f , if the DNP expresses the ground state accurately, the reweighting function $f(s)$ satisfies

$$p(s) = \frac{f(s)}{Z} q(s), \quad Z = \sum_s f(s)q(s), \quad (16)$$

and the *dynamical range* of the DNP is quantified as

$$\gamma = \frac{\max_s f(s)}{\min_s f(s)} \leq r^2. \quad (17)$$

The range γ measures how strongly the post-processing must rescale the Born probabilities of the ansatz to reproduce the target distribution. If γ must grow exponentially with the number of qubits, then either the neural-network parameters or the required measurement count must also scale exponentially to resolve such reweighting, implying an intrinsic overhead in accuracy.

We express the classical fidelity of the probability distributions, $p(s)$ and $q(s)$, via the Bhattacharyya coefficient,

$$B(p, q) = \sum_s \sqrt{p(s)q(s)}. \quad (18)$$

For the Born distributions of two quantum states, it can also be viewed as the square-root of the fidelity between two pure states.

Meanwhile, we consider the Rényi- $\frac{1}{2}$ divergence and the Rényi- ∞ divergence, which obey the monotonicity

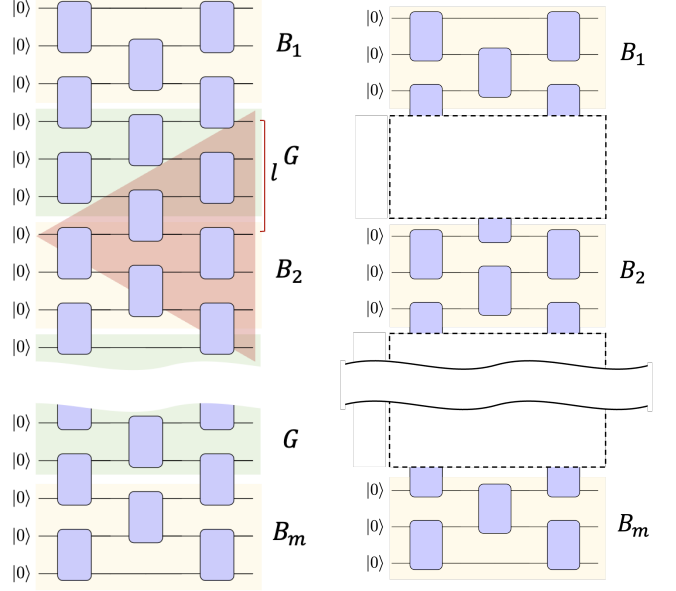


FIG. 2: Sketch of proof of exponential decay of Bhattacharyya coefficient in a finite-depth circuit. Each layer acts locally on neighboring qubits, forming a backward light-cone (red wedge) of finite width $\ell = O(d)$. (a) The circuit is divided into blocks B_i , with buffer regions in between each pair of blocks of length $g \gtrsim \ell$. Because this light-cone remains bounded as the total system size grows, the Bhattacharyya coefficient between two independently drawn circuit outputs approximately factorizes across independent blocks, leading to the exponential decay. (b) The buffer region has been discarded via classical stochastic channel. The remaining blocks have almost no overlap to the other blocks. The formal proof can be found in Appendix C.

property

$$D_{1/2}(p\|q) \leq D_\infty(p\|q), \quad (19)$$

see Appendix C for precise definitions. For the DNP transformation $p(s) = f(s)q(s)/Z$, one finds

$$\begin{aligned} D_\infty(p\|q) &= \log \max_s f(s) - \log Z, \\ D_\infty(q\|p) &= -\log \min_s f(s) + \log Z, \end{aligned} \quad (20)$$

by inserting $p(s)$ into the expression for D_∞ , which is also given in Appendix C. Together, they yield the general inequality

$$\gamma = \frac{\max_s f(s)}{\min_s f(s)} \geq B(p, q)^{-4}. \quad (21)$$

Hence, the required dynamic range γ is inversely related to the overlap of the ansatz and target distributions. If $B(p, q)$ decays exponentially with the system size, the reweighting function $f(s)$ must exhibit an exponentially

large dynamic range, even under bounded neural activations.

For constant-depth circuits of circuit depth d , the output distribution $q(s)$ possesses a finite light-cone length $\ell = O(d)$ and limited correlation range, as shown in Fig. 2 (a). The system can be partitioned into nearly independent blocks of size $L \gtrsim \ell$, each contributing a finite local mismatch to the global distribution. If the local Rényi- $\frac{1}{2}$ gap on each block is bounded below by a positive constant $\delta^* > 0$, the global Bhattacharyya coefficient decays exponentially with n , formally stated in the following theorem.

Theorem 1 (Exponential decay of the Bhattacharyya coefficient). *Suppose there exists a block size $L = O(d)$ and a constant $\delta^* > 0$ such that, for every contiguous block of L qubits, the local Rényi- $\frac{1}{2}$ divergence between the corresponding marginals of p and q is bounded below by δ^* . Then the Bhattacharyya coefficient between p and q decays exponentially with n :*

$$B(p, q) \leq \exp\left(-\frac{\delta^*}{4L} n\right). \quad (22)$$

Proof sketch. —The argument exploits the finite light-cone of a depth- d local circuit. Partition the n qubits into blocks of size $L = O(d)$ separated by buffer regions larger than the light-cone. Discarding (tracing out) the buffers defines a classical stochastic map under which the Rényi- $\frac{1}{2}$ divergence cannot increase. Locality implies that, after discarding the buffers, the ansatz distribution approximately factorizes across blocks, so the Rényi- $\frac{1}{2}$ divergence becomes (approximately) additive over blocks. A uniform local gap δ^* on each block therefore accumulates linearly in the number of blocks, yielding $D_{1/2}(p\|q) = \Omega(n)$. Using $B(p, q) = \exp[-D_{1/2}(p\|q)/2]$ gives Eq. (22). A complete proof (including the control of buffer-induced approximation errors) is given in Appendix C. \square

Intuitively, the exponential overhead stems from the mismatch between the ansatz distribution and the true ground-state distribution. As the system size increases, this mismatch worsens due to the limited expressiveness of a finite-depth parametrized quantum circuit. This limitation is fundamental: if approximating the target distribution requires an exponentially growing dynamic range in the neural network output, then classical post-processing with polynomially scaling resources cannot serve as a general remedy for the expressibility bottleneck in variational quantum algorithms.

D. Exponential resource requirement of constrained DNP: linear-depth circuits

The exponential decay of the Bhattacharyya coefficient for finite-depth circuits raises the question of whether increasing the circuit depth can overcome this limitation. Unfortunately, once the depth scales linearly with system size, the ansatz enters the barren-plateau regime [26, 27]:

its parameter landscape becomes exponentially concentrated and gradients vanish with n , rendering optimization intractable for large systems. Such circuits form approximate unitary 2-designs [28], meaning that their output distributions in the computational basis reproduce the first two moments of Haar-random ensembles.

In this regime, the Born distribution $q(s) = |\langle s|\psi_0 \rangle|^2$ behaves statistically like a Haar-random sample, with amplitudes delocalized over the 2^n -dimensional Hilbert space. By concentration of measure (e.g., Lévy's lemma) and the Dirichlet statistics of Haar amplitudes, the classical overlap between a 2-design circuit and any fixed target distribution also decays exponentially.

Theorem 2 (Bhattacharyya coefficient for unitary 2-design states). *Let $|\psi\rangle \in \mathbb{C}^{2^n}$ be a pure state following unitary 2-design with measurement probabilities $q(s) = |\langle s|\psi \rangle|^2$. For a fixed quantum state $|\phi_0\rangle$ and its probability distribution $p(s) = |\langle s|\phi_0 \rangle|^2$, it holds that*

$$B(p, q) = \Theta(2^{-n/2}), \quad (23)$$

with probability $1 - e^{-\Omega(2^n)}$.

Proof sketch. —For Haar-random states (and hence for unitary 2-design ensembles), the vector of computational-basis probabilities follows a symmetric Dirichlet distribution. A direct Beta-moment calculation gives $\mathbb{E}[\sqrt{q(s)}] = \Theta(2^{-n/2})$ for each bit string s , and therefore $\mathbb{E}[B(p, q)] = \sum_s \sqrt{p(s)} \mathbb{E}[\sqrt{q(s)}] = \Theta(2^{-n/2})$ up to a p -dependent prefactor. Concentration of measure (e.g., Lévy's lemma) then shows that $B(p, q)$ concentrates exponentially around its mean, yielding the stated scaling with probability $1 - e^{-\Omega(2^n)}$. Full details are provided in Appendix D. \square

Substituting Eq. (23) into the general dynamical-range bound $\gamma \geq B^{-4}$ [Eq. (21)] yields

$$\gamma \geq \Omega(2^{2n}), \quad (24)$$

up to a constant prefactor dependent on p . Thus, even though linear-depth circuits explore exponentially large subspaces, their typical overlap with the desired ground-state distribution is exponentially small.

Consequently, irrespective of the ansatz depth—whether it is constant depth (remaining trainable in the large-qubit regime but lacking expressiveness) or linear depth (offering better ground-state approximations but incurring exponential training cost)—the neural network must have sufficient expressive capacity to cover a wide range of output values in order to reproduce the ground state with arbitrary precision. However, as discussed earlier, expanding this dynamical range inevitably increases the required number of measurements. Therefore, combining DNP with conventional variational ansatzes cannot simultaneously achieve both accuracy and efficiency.

Corollary 1 (Resource-consistency obstruction for DNP). *Consider a DNP-based post-processing protocol*

that is trained on-device without prior knowledge (Definition. 1). To (i) prevent the empirical objective from becoming unbounded below one must, in general, enforce the support-inclusion event $B_M \subseteq B_a$, which requires exponentially many ansatz shots even in the most favorable uniform case (Prop. 2). Moreover, to (ii) approximate the ground-state energy within constant precision using either constant-depth ansatzes satisfying the locality condition of Theorem 1 or linear-depth ansatzes in the unitary 2-design regime of Theorem 2, the required reweighting range r grows exponentially with n . Combined with the shot-complexity bound (15), this implies an exponential measurement cost. Consequently, DNP cannot simultaneously satisfy polynomial resources and variational consistency in the large-system limit.

Proof sketch. —For variational consistency under finite sampling, one must keep the empirical ratio objective well-posed. Proposition 1 shows that if $B_M \not\subseteq B_a$, then (in general) the empirical DNP objective can be driven to $-\infty$ by amplifying weights on unseen configurations, so avoiding this failure mode requires enforcing (or effectively approximating) support inclusion. Proposition 2 shows that even in the most favorable uniform-ansatz setting, ensuring $B_M \subseteq B_a$ with constant success probability costs exponentially many ansatz shots when $|B_M|$ grows exponentially with n .

For accuracy at constant precision, Theorem 1 (constant-depth ansatzes) and Theorem 2 (2-design regime) imply that the dynamic range required to reproduce the ground-state distribution—and hence the admissible bound parameter r —must grow exponentially with n . Combining this with the shot requirement Eq. (15) for stable estimation under bounded outputs forces an exponential measurement cost. Together, these implications rule out simultaneously achieving polynomial resources and variational consistency for DNP in the large-system limit under self-contained training. \square

IV. TRAINING NEURAL NETWORK IN PRACTICAL SCALE MEASUREMENT REGIME

Although the previous section established that DNP-style algorithms inherently require exponential resources—whether quantum or classical—they can still be used to enhance the performance of standard VQE in practical settings. In this section, we examine the training behavior of DNP-style algorithms via VQNHE, focusing on neural-network dynamics under practical resource scaling. By varying the number of measurement shots N , the dynamical range r of the neural-network outputs, and the number of qubits n , we analyze how and why the DNP algorithm exhibits distinct behaviors across these regimes.

DNP constraints and expressiveness Fig. 3(a)–(c) illustrates the impact of neural-network constraints on the expressiveness of DNP algorithms. Most notably, it shows that across all system sizes, increasing r (and

the corresponding number of measurements (15)) pushes the estimated energy closer to the exact ground-state energy. This trend can be interpreted in terms of both the measurement budget and the constraint parameter r .

Naturally, as r increases—allowing the neural network to represent a broader range of output values—the network gains the ability to explore a wider solution space beyond what the trained ansatz alone can reach. Although achieving arbitrarily precise results would, as shown earlier, require an exponentially growing dynamical range with system size, in practice it is often most effective to choose r as large as possible within the limits of available measurement resources.

The role of the dynamical range in the expressiveness of DNP can also be seen in a fixed-shot setting, as shown in Fig. 3(d). Provided that sufficient measurements are taken to prevent the instabilities discussed below, increasing r enhances expressiveness, allowing the estimator to approximate the exact ground-state energy more closely.

Falling below the ground-state energy Even with constrained DNP, however, one cannot prevent the estimate from falling below the exact ground-state energy. This phenomenon stems from the need for normalization and inevitable measurement error. Without prior knowledge of the ground state or its energy, the neural network is tasked solely with minimizing the loss function. However, due to the inherent mismatch between the sets of measured bit strings contributing to the numerator \hat{N}_f and denominator \hat{Z}_f , the network can artificially lower the loss by assigning extremely large (small) values to bit strings that appear only in the numerator (denominator). Although such behavior does not guide the optimization toward the true ground state, it nonetheless satisfies the formal objective of minimizing the loss function. This manipulation effectively distorts the normalization: adjusting weights on these specific bit strings influences only one of the two estimators—either the numerator or the denominator—thereby breaking their balance.

Figure 3(e) illustrates how increasing r can distort the normalization, leading to nonphysical deviations below the true ground-state energy. As discussed, this improper normalization arises when the neural network assigns extreme values to a subset of bit strings—an effect that becomes more pronounced as the dynamical range r grows. In contrast to Fig. 3(d), where larger r values improve accuracy given sufficient measurement shots, increasing r can deteriorate performance when normalization errors arise due to missing bit-string support in the measured bit strings. The divergence observed in Fig. 1(a) is an extreme manifestation of this behavior under unconstrained DNP. In summary, although a larger dynamical range enhances expressiveness and can, in principle, enable closer approximation to the exact ground state, limited measurement resources can cause DNP to produce nonphysical results, potentially leading to critical misinterpretations of the system’s behavior.

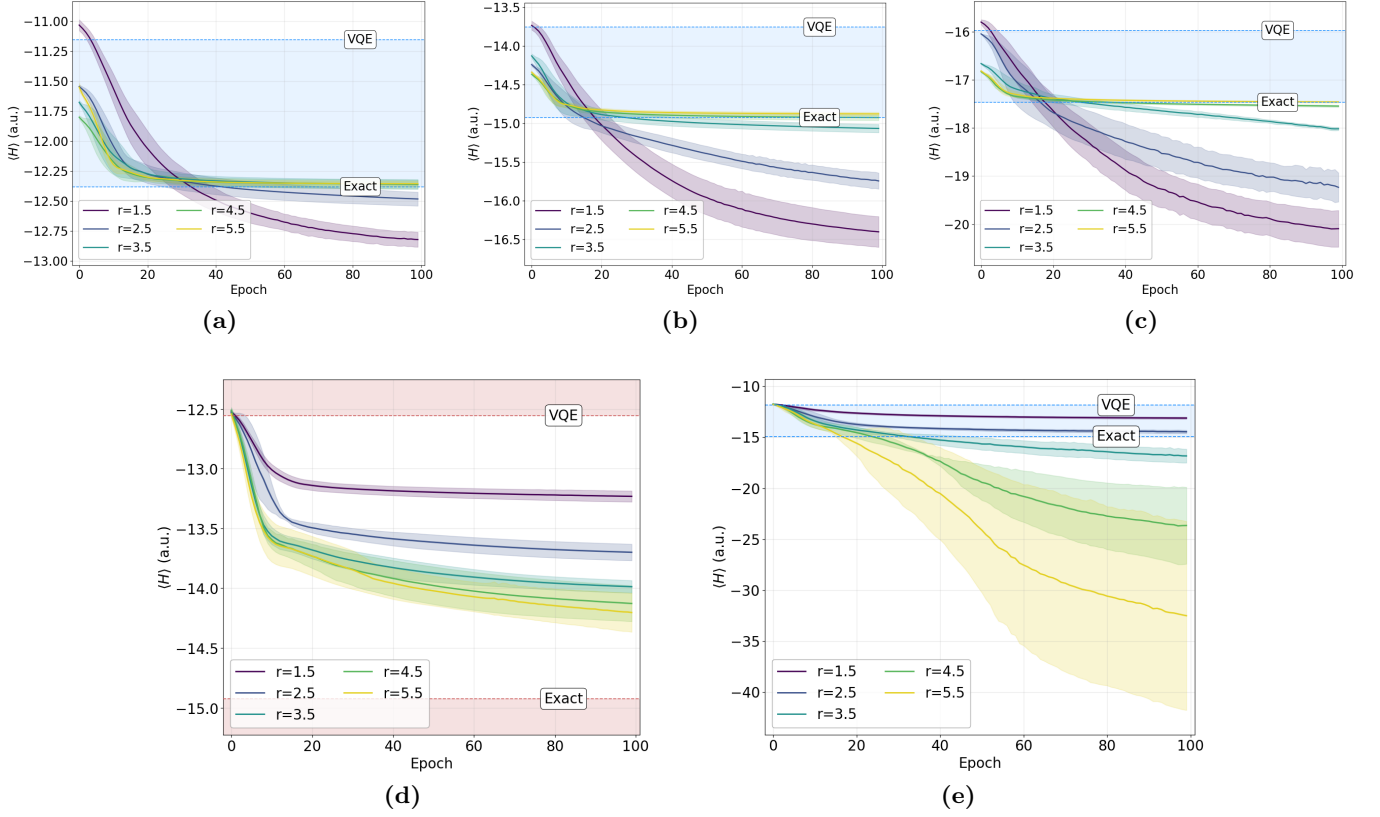


FIG. 3: Training curves of the neural network in VQNHE with constraints applied, for transverse-field Ising models of various sizes and shot numbers. (a)–(c) show 10-, 12-, and 14-qubit systems, respectively, where the neural-network output is constrained to $f(s) \in [1/r, r]$ for r values from 1.5 to 5.5. For each r , the number of circuit shots is set to $N = \frac{9r^4}{4\epsilon^2}$ [23], ensuring deviations smaller than $\epsilon = 0.05$. The shaded blue regions indicate the range between the VQE baseline and the exact ground-state energy. (d)–(e) correspond to 12-qubit systems trained under fixed-shot conditions: (d) $N = 135,056$ shots per circuit, satisfying the accuracy bound at $r = 3.5$, and (e) $N = 10,000$ shots per circuit. In these plots, the shaded red or blue regions indicate the area between the VQE baseline and the exact energy.

System size dependence Figure 4(a) shows the deviation between the VQNHE results obtained with fixed computational resources and the exact ground-state energies of the TFIM. Since the dynamical range of the neural network is fixed, the expressiveness of DNP is likewise limited, and one might intuitively expect the deviation from the exact solution to grow with system size. However, as shown in the figure, the deviation becomes increasingly negative as the number of qubits grows, indicating not only a systematic deterioration in accuracy, but also that the solution is nonphysical. This worsening trend highlights the difficulty of scaling DNP to larger systems under fixed resource conditions, consistent with the exponential scaling required—either in the number of measurements or in the dynamical range—to maintain accuracy.

In conclusion, the DNP framework exhibits several noteworthy behaviors during neural-network training. First, when a sufficient number of measurement shots are available—though beyond the polynomial-resource regime—a wider output range of the neural network

enables a more accurate approximation to the ground-state energy. In contrast, within the polynomial-shot regime, increasing the dynamical range can degrade performance, often producing nonphysical energies below the true ground-state value due to normalization issues. This deviation becomes progressively more severe as the number of qubits increases, reflecting the growing difficulty of maintaining stability under limited measurement resources.

V. STABLE TRAINING VIA UNITARY POST-PROCESSING

The previous Sec. II C–III show that the explicit normalization intrinsic to DNP is not a benign implementation detail: under finite sampling, normalization turns the DNP objective into a ratio estimator whose value can be dominated by rare configurations. As a consequence, the polynomial measurement budgets can lead to support mismatch between numerator and denominator es-

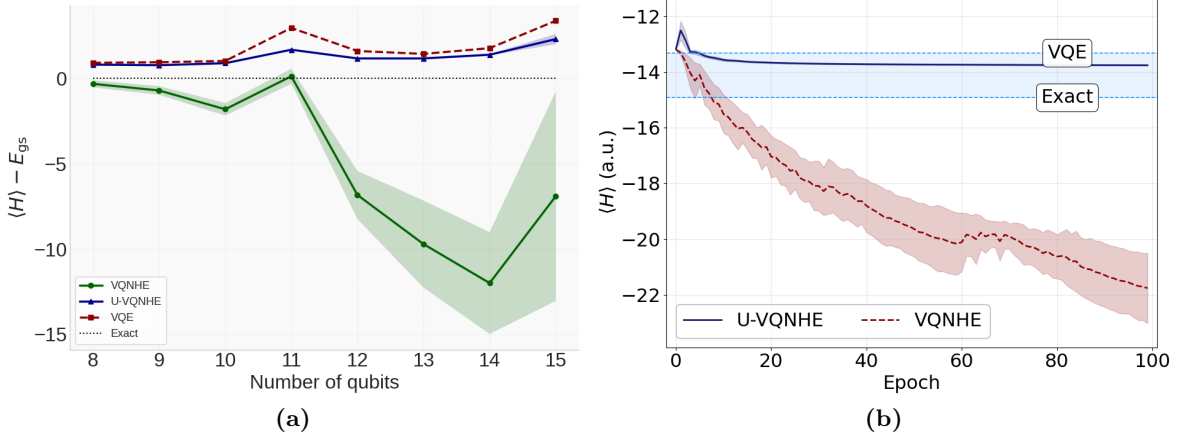


FIG. 4: Comparison of the training performance of VQNHE and U-VQNHE. (a) Energy difference from the ground-state energy for TFIM instances with increasing numbers of qubits, using 10,000 measurements per circuit. The neural-network output is bounded within $[1/3, 3]$, as before. The red dashed line shows the gap between VQE and the ground-state energy. As the number of qubits increases, the deviation between VQNHE and the exact ground-state energy generally worsens. (b) Results for a 12-site TFIM using a two-layer ansatz and 10,000 measurements per circuit. The region between the exact ground-state energy and the VQE result is shown in light blue. The solid blue line shows the result from U-VQNHE, while the dotted red line shows that of VQNHE with constrained DNP (with range parameter $r = 3$). VQNHE violates the variational bound, leading to nonphysical solutions, whereas U-VQNHE remains within the physical region while improving upon VQE.

timators (Sec. III), and the empirical loss landscape may develop nonphysical directions that violate the Rayleigh–Ritz bound. This motivates a simple design principle for quantum-neural hybridization to preserve the normalization by construction. If the post-processing layer is norm-preserving, then (in the absence of additional noise) its objective is automatically the expectation value of H on a valid quantum state, and variational consistency follows immediately.

We implement this principle by replacing the diagonal non-unitary filter D_f with a diagonal unitary transformation. A diagonal map is unitary if and only if each diagonal entry has unit modulus. Hence, instead of learning amplitudes $f(s) \in \mathbb{R}$ as in DNP, we let the neural network output a real-valued phase function $g_\phi(s) \in \mathbb{R}$ and define the diagonal unitary

$$|\psi_u(\theta)\rangle = U_g |\psi(\theta)\rangle, \quad U_g = \sum_{s \in \{0,1\}^n} e^{ig_\phi(s)} |s\rangle\langle s|. \quad (25)$$

This phase-only post-processing is compatible with the complex-valued formulation discussed in the supplementary material of Ref. [23], but crucially it eliminates the need for explicit (and sampling-limited) renormalization.

Theorem 3 (Variational safety of diagonal unitary post-processing). *Let $U_g = \sum_{x \in \Omega} e^{ig(x)} |x\rangle\langle x|$ be a diagonal unitary defined by an arbitrary real-valued function $g : \Omega \rightarrow \mathbb{R}$. For any normalized ansatz state $|\psi(\theta)\rangle$, the post-processed state $|\psi_u(\theta)\rangle = U_g |\psi(\theta)\rangle$ is normalized and satisfies the Rayleigh–Ritz bound*

$$\langle \psi_u(\theta) | H | \psi_u(\theta) \rangle \geq E_{\text{gs}}. \quad (26)$$

In particular, any exact evaluation of the U-VQNHE objective is variationally consistent by construction.

Proof. —The unitarity of U_g implies $\|\psi_u(\theta)\| = \|\psi(\theta)\| = 1$. The Rayleigh–Ritz principle then gives $\langle \psi_u | H | \psi_u \rangle \geq E_{\text{gs}}$ for any normalized state $|\psi_u\rangle$. \square

Operationally, U-VQNHE inherits the circuit-transformation estimator of VQNHE: the diagonal unitary U_g is applied only virtually through classical post-processing of measurement outcomes. Because the learned phase factors introduce complex interference, estimating $\langle \psi_u | P | \psi_u \rangle$ requires access to both real and imaginary parts; this can be achieved by at most doubling the set of measurement circuits used in VQNHE. Importantly, the estimator remains linear in shot-averaged quantities and does not involve an explicit normalization ratio. Derived directly from VQNHE, the expectation value from this transformed state is evaluated as

$$\begin{aligned} \langle \hat{H} \rangle_g &= \sum_P c_P \left[\sum_{s \in B_{m,P}} (-1)^{q^*} \text{Re} \left(e^{-ig(s')} e^{ig(\tilde{s}'_P)} \right) p_m(s; P) \right. \\ &\quad \left. + \sum_{s \in B_{m',P}} (-1)^{q^*} \text{Im} \left(e^{-ig(s')} e^{ig(\tilde{s}'_P)} \right) p_{m'}(s; P) \right]. \quad (27) \end{aligned}$$

Here, $p_m(s; P)$ is the probability distribution of the measurement circuits of VQNHE, and $p_{m'}(s; P)$ is that of the measurement circuits corresponding to the imaginary parts. The total number of measurement circuits that must be evaluated is at most doubled, but none of them

requires exponential number of shots, nor does the algorithm require normalization circuit.

Fig 4 shows how U-VQNHE compares to the non-unitary counterpart. As the results suggest, the key advantage of U-VQNHE over DNP algorithms is that it satisfies the third requirement of staying within the Rayleigh-Ritz variational bound. Due to the nature of the unitary transformation, the transformed state $|\psi_u\rangle$ always represents a physical solution with a closer eigenenergy compared to the one from the standard VQE.

VI. DISCUSSIONS AND OUTLOOKS

The central message of this work is that how one hybridizes the variational quantum algorithms with classical neural network matters as much as whether one hybridizes them. The diagonal neural post-processing (DNP) has been appealing because it is simple, expressive, and classically lightweight. It learns a bit-string-dependent rule that reshapes the effective objective of VQE while keeping the quantum circuit fixed. Our analysis shows, however, that the very feature that enables this flexibility—a non-unitary, amplitude-changing filter followed by explicit normalization—creates an intrinsic statistical failure mode under finite sampling. In the DNP objective, the errors in the estimated normalization enter multiplicatively through a ratio, and a small set of rare configurations can dominate the loss. This leads to two intertwined obstructions: (i) with sub-exponential shots the empirical loss can become ill-conditioned and even sub-variational (Secs. III and IV), and (ii) even when one constrains the network output to stabilize training, accurately reproducing the ground state generically requires an exponentially large reweighting range (Theorems 1 and 2).

From a physics perspective, these results highlight a useful way to interpret “variational safety.” In standard VQE, the reported number is always $\langle\psi|H|\psi\rangle$ for a normalized state $|\psi\rangle$, so the Rayleigh–Ritz bound is a built-in sanity check. DNP breaks this direct link: at finite shots one optimizes an empirical ratio \hat{E}_f that need not correspond to any normalized state at all. The resulting sub-variational energies are therefore not simply “overfitting” in the machine-learning sense; they are symptoms of an estimator that has escaped the variational manifold because normalization was inferred, imperfectly, from incomplete samples. In this sense, the breakdown is architectural rather than parametric: it is not resolved by better optimizers or mild regularization, but requires changing the normalization logic itself.

The constructive counterpart of our no-go result is the design principle used in Sec. V: i.e., enforce norm preservation by construction. Our diagonal unitary post-processing is the minimal realization of this principle. Because it preserves the norm exactly, it restores the direct variational interpretation of the objective (Theorem 3) while retaining the practical workflow of a learnable diag-

onal layer implemented through classical post-processing. At the same time, the unitary restriction makes clear what is and is not being learned: unlike DNP, a diagonal unitary cannot change Born probabilities in the computational basis, and therefore cannot emulate arbitrary amplitude filters. Rather, it learns a phase landscape that can still affect energies through interference in the measurement bases required for Pauli terms. Our numerical experiments suggest that this phase degree of freedom is already sufficient to obtain a robust improvement over VQE in relevant regimes, without ever sacrificing variational consistency.

Several directions are opened by the present work. First, it is natural to ask how far the “norm-by-construction” principle can be pushed beyond diagonal unitaries, for example by learning shallow unitary post-processing circuits or by using trace-preserving quantum channels whose classical description remains efficient. Second, the resource obstruction we identify for DNP can be viewed through the lens of variance control for ratio estimators: developing hybrid objectives that avoid explicit normalization (or that control it with provable concentration guarantees) may yield new, statistically well-behaved learning interfaces for quantum devices. Finally, U-VQNHE can be combined with orthogonal improvements to VQE—such as adaptive ansatz growth, symmetry constraints, or subspace-expansion techniques—to explore whether phase-learning post-processing provides complementary benefits in larger and more structured Hamiltonians. We hope that the rigorous characterization given here helps clarify which hybridization strategies are likely to scale, and which are destined to fail for fundamental statistical reasons.

VII. ACKNOWLEDGMENTS

This work has been supported by the National Research Foundation of Korea (NRF) grant (No. RS-2024-00442855, No. RS-2024-00413957, No. RS-2024-00432214, and No. RS-2025-18362970), and the Institute of Information & Communications Technology Planning & Evaluation (IITP) grant (No. RS-2022-II221040), all of which are funded by the Korean government (MSIT).

VIII. AUTHOR CONTRIBUTIONS

M.K. conceived the project, identified the issues, proposed the algorithm, developed the mathematical framework, and wrote the manuscript. K.P. and K. L. provided guidance on the project and feedback on the manuscript. The simulation code was implemented by M.K.. J.B. and T.K. supervised the project, including research planning and manuscript preparation. We also thank Luning Zhao for mentoring and helpful discussions.

IX. CODE AVAILABILITY

Python scripts that generate all figures and execute the algorithms are archived at Github, <https://github.com/minukim/vqnhelb>.

Appendix A: Variational Quantum-Neural Hybrid Eigensolver

VQNHE [23] augments a standard VQE by inserting a diagonal non-unitary post-processing

$$D_f = \sum_{s \in \{0,1\}^n} f(s) |s\rangle\langle s|, \quad (\text{A1})$$

that reweights measurement outcomes of a variational state $|\psi\rangle$. This is a standard setting of DNP where we have $\Omega = \{0,1\}^n$ and $x = s$. The reweighting converts Born probabilities $p_\psi(s) = |\langle s | \psi \rangle|^2$ into $p_f(s) \propto |f(s)|^2 p_\psi(s)$, increasing the effective expressiveness of a shallow ansatz without changing its circuit structure.

Let $\hat{H} = \sum_P c_P P$ with Pauli strings P . For each P , choose a *star qubit* q_* within the support of the X/Y factors of P . For every other qubit j in the X/Y support of P with $j \neq q_*$, apply a controlled gate onto q_* with control j : use controlled- X if P has X on j and controlled- Y if P has Y on j . This aggregates the X/Y -parity of P onto the star qubit. After this aggregation, perform the standard computational-basis diagonalization for P : apply H on qubits where P has X , $R_X(-\pi/2)$ on qubits where P has Y , and measure directly where P has Z or I . A final computational-basis readout then yields bit strings $s = (s_*, \bar{s})$, and the eigenvalue of P is encoded in the star-qubit outcome via $\sigma_P(s) = (-1)^{s_*}$.

Let $f : \{0,1\}^n \rightarrow \mathbb{C}$ define D_f as above. Denote by $p_P(s)$ the shot-normalized probability of s obtained from the circuit used to measure P , and by $p_I(s) = p_\psi(s)$ the probability from the bare ansatz circuit, or equivalently from the Pauli term I . The chosen diagonalization of P induces a deterministic map $s \mapsto \tilde{s}_P$ on data bit strings such that it exerts XOR operations on the support of X and Y . For example, if $P = XYZ$, $s = 011$, then $\tilde{s}_P = 101$. Also define a filter $s \mapsto s'$ that sets the star-qubit bit of s to 0 in s' while leaving all other bits unchanged, or in other words, $s = (s_*, \bar{s}) \mapsto s' = (1 \oplus s_*, \bar{s})$.

With these definitions, the energy estimator reads

$$\langle \hat{H} \rangle_f = \frac{\sum_P c_P \sum_{s=(s_*, \bar{s})} f(s') f(\tilde{s}'_P) \sigma_P(s) p_P(s)}{\sum_s |f(s)|^2 p_I(s)}. \quad (\text{A2})$$

In practice, the sums are implemented as Monte Carlo averages over the corresponding shot ensembles: the numerator averages $c_P f(s'_i) f(\tilde{s}'_{P,i}) \sigma_P(s_i)$ over samples s_i drawn from the P -measurement circuits, while the denominator averages $|f(t_j)|^2$ over samples t_j drawn from

the ansatz circuit itself, or with respect to the identity term. Equation (A2) makes explicit that the quantum hardware supplies unweighted bit strings and all diagonal reweighting is performed in classical post-processing via D_f .

Appendix B: Neural post processing algorithms from the DNP framework

In this appendix we detail how several descendants of the variational quantum–neural family operate in practice and how each can be written as an expansion of the DNP map

$$\mathcal{D}_f(\rho) = \frac{D_f \rho D_f^\dagger}{\text{Tr}[D_f \rho D_f^\dagger]}, \quad D_f = \sum_{x \in \Omega} f(x) |x\rangle\langle x|,$$

where x denotes the measurement record used in post-processing and Ω is its domain. Throughout, the underlying variational state is $|\psi(\boldsymbol{\theta})\rangle = U(\boldsymbol{\theta}) |0\rangle^{\otimes n}$ (or, when additional measured registers are present, the corresponding state on the enlarged register), and the post-processed state is

$$|\tilde{\psi}(\boldsymbol{\theta})\rangle_f = \frac{D_f |\psi(\boldsymbol{\theta})\rangle}{\|D_f |\psi(\boldsymbol{\theta})\rangle\|},$$

with

$$\|D_f |\psi(\boldsymbol{\theta})\rangle\| = \sqrt{\langle \psi(\boldsymbol{\theta}) | D_f^\dagger D_f | \psi(\boldsymbol{\theta}) \rangle}.$$

1. Variational post-selection

Variational post-selection [29] augments a variational state with one or more ancilla qubits. After state preparation, measurement outcomes are *filtered* before forming expectation values, thereby biasing the effective sample distribution toward a target subspace or target statistics while preserving a normalized estimator. In the ground-state setting this filtering is implemented by projecting onto a designated set of accepted ancilla outcomes, while in the thermal-state setting it is implemented via a graded acceptance profile $g \in [0, 1]$, i.e., a neural reweighting of ancilla outcomes prior to normalization.

At the density-matrix level, let the joint system–ancilla state be $|\Psi\rangle = \sum_{i,m} \psi_{im} |i\rangle_{\text{sys}} |m\rangle_{\text{anc}}$. Reweighting the ancilla outcome m by $g(m)$ and tracing out the ancilla yields the reduced system state

$$\rho_{ij}^{(\text{sys})}(g) \propto \sum_m \psi_{im} g(m) \psi_{jm}^*, \quad (\text{B1})$$

which specializes to projector-based post-selection when g is an indicator on the accepted ancilla set.

From the DNP viewpoint, this is a diagonal, non-unitary post-processing on the extended measurement

record $x = (s, m) \in \Omega$, with $\Omega = \{0, 1\}^n \times \mathcal{M}$, implemented by

$$D_{f_{\text{ext}}} = \sum_{s, m} f_{\text{ext}}(s, m) |s, m\rangle\langle s, m|, \quad (\text{B2})$$

$$f_{\text{ext}}(s, m) = \sqrt{g(m)} f(s),$$

followed by the usual DNP renormalization. In other words, variational post-selection remains within DNP by enlarging the outcome domain and absorbing the post-selection (or neural acceptance) into the diagonal weights.

2. pUNN

Relative to standard DNP, which applies a diagonal weight $f(s)$ to single-register bit strings, paired unitary coupled-cluster with neural networks (pUNN) enlarges the space on which the diagonal weights act [30]. In the DNP definition, this corresponds to replacing the outcome domain $\Omega = \{0, 1\}^n$ by a product domain $\Omega = \mathcal{K} \times \mathcal{J}$ and applying a diagonal, non-unitary weight function $F(k, j)$ on the joint measurement record $x = (k, j)$. Concretely, pUNN pairs the paired unitary coupled-cluster with double excitations ansatz [31] with an auxiliary circuit of the same size where classical perturbation is given before it is entangled with the system, and lets the diagonal weight depend on both indices, $F : \mathcal{K} \times \mathcal{J} \rightarrow \mathbb{R}$ (or \mathbb{C}). This lift gives the model enough capacity to encode correlations that a single-index $f(s)$ cannot.

Under this viewpoint, pUNN is simply DNP on the enlarged register, with diagonal operator

$$D_F = \sum_{(k, j) \in \mathcal{K} \times \mathcal{J}} F(k, j) |k, j\rangle\langle k, j|,$$

and the energy is then computed using the same normalized estimator structure as DNP. Operationally, the auxiliary tag j gives the neural post-processing an extra conditioning variable. This allows pUNN to represent reweightings that cannot be captured by a function of the hardware outcome k alone—intuitively, it can learn different reweighting rules for the same k depending on the accompanying tag j , thereby encoding additional correlations.

If one averages over the auxiliary tag, the scheme collapses back to an effective single-variable reweighting on k , recovering standard DNP in form. Keeping the pair (k, j) explicit is therefore the distinguishing feature of pUNN: it is best viewed as DNP applied to an enlarged outcome space, with the same ratio-of-expectations structure but a richer input domain for the diagonal weights.

3. sVQNHE

Signed-VQNHE (sVQNHE) [25] builds on diagonal neural post-processing, but modifies the hybrid design and training procedure to more explicitly accommodate sign/phase structure. Within our DNP definition, sVQNHE retains the same measurement-outcome domain (typically $\Omega = \{0, 1\}^n$) and the same diagonal reweighting layer specified by a neural network f acting on bit strings, while enforcing additional restrictions on the admissible outputs of f (and associated regularization) to improve numerical conditioning and reduce estimator variance. In parallel, sVQNHE assigns the learning of sign/phase information to the quantum circuit by incorporating commuting diagonal gates, which provide a structured and measurement-efficient mechanism for encoding phases beyond what the diagonal neural reweighting alone can capture.

Operationally, sVQNHE employs a layer-wise, phase-amplitude decoupling strategy with a bidirectional feedback loop between the neural network and the PQC. At each iteration, a new block of quantum layers is added: a classically simulatable, non-diagonal layer (used to shape amplitudes) together with a diagonal layer (used to learn phases). The algorithm first performs a forward initialization step, where the amplitude structure learned by the neural operator from the previous iteration is transferred to the newly added simulatable layer via a tractable classical optimization. Then, in the subsequent hybrid optimization step, the neural operator is reset and jointly optimized together with the parameters of the new diagonal layer, following the same variational objective as in basic DNP. Leveraging the commuting nature of the diagonal layers, sVQNHE is designed to reduce measurement overhead for updating the phase-related parameters, while retaining the DNP component as the amplitude-learning module. Furthermore, they argue that their layer-wise structure mitigates normalization issues, which is mainly addressed in our paper to be inherent in DNP structure.

4. VQNHE++

The three variants above remain *within* the DNP abstraction in the strict sense that they only modify the diagonal weight function (and/or its domain) while preserving the same post-processing map $\mathcal{D}_f(\rho) = D_f \rho D_f^\dagger / \text{Tr}[D_f \rho D_f^\dagger]$ and the same normalized ratio estimator. By contrast, VQNHE++ [32] should be viewed as a *DNP-based extension*: it retains the DNP layer unchanged, but augments the overall procedure with an additional classical degree of freedom that acts on the Hamiltonian representation.

In the DNP setting we keep the quantum state preparation fixed within a measurement round, collect rotated-basis histograms that diagonalize each Hamilto-

nian term, and apply a diagonal (generally non-unitary) post-processing $D_f = \sum_s f(s) |s\rangle\langle s|$ (equivalently, $x = s \in \Omega = \{0, 1\}^n$). The energy is evaluated as introduced in Eq. A2, where $H = \sum_P c_P P$, $p(t) = |\langle t|\psi\rangle|^2$ is the bare-ansatz distribution, $p_P(s)$ is the distribution from the circuit used to measure P , $s \mapsto s'$ is the star-collapse map that sets the star bit to 0, \tilde{s}'_P is the companion bit string induced by the chosen diagonalization of P , and $\sigma_P(s) = (-1)^{s'}$ is the eigenvalue sign read from the star qubit.

VQNHE++ introduces a tunable gauge W_τ and tracks the transformed Hamiltonian

$$H_\tau = W_\tau^\dagger H W_\tau, \quad (\text{B3})$$

on the operator side. Practically, this means that the coefficients used to compile the DNP estimator become τ -dependent. Crucially, however, once τ is fixed, the subsequent estimation step is exactly the same as standard DNP applied to the same measurement data: the measurement pipeline and the diagonal reweighting by f remain unchanged, and the energy is still computed as the same normalized ratio-of-expectations, but now with the Pauli expansion and associated tables taken from H_τ rather than H .

This perspective makes the algorithmic structure explicit: VQNHE++ composes a classical transformation module with a DNP evaluator, so that DNP appears as a subroutine inside a larger variational loop. When optimizing for a fixed Hamiltonian, VQNHE++ reduces to VQNHE as soon as τ is fixed: the DNP code sees constant operator-side coefficients and the optimization over f (and any circuit parameters) is precisely the original form. More generally, one may alternate between updating (θ, f) at fixed τ (pure DNP on a fixed operator representation) and updating τ at fixed (θ, f) , or co-optimize them if desired.

To absorb both ideas into an existing DNP implementation: (i) given τ , regenerate the operator-side coefficients from H_τ ; then (ii) call the same DNP estimator/evaluator with those tables and the same diagonal weights. In all cases, the core non-unitary post-processing and the normalization-dependent ratio structure remain unchanged; VQNHE++ augments DNP by adding a classical, variational transformation of the Hamiltonian representation.

Appendix C: Proof of exponential decay of Bhattacharyya coefficient: constant-depth circuits

In this appendix, we prove exponential decay of the Bhattacharyya coefficient between finite-depth circuit and the ground state. First, we define several relevant concepts.

For two probability distributions p and q on the same finite sample space, the Rényi divergence of order $\alpha \in$

$(0, \infty) \setminus \{1\}$ is

$$D_\alpha(p\|q) = \frac{1}{\alpha-1} \log \left(\sum_x p(x)^\alpha q(x)^{1-\alpha} \right). \quad (\text{C1})$$

[33] In particular, the Rényi- $\frac{1}{2}$ divergence can be written in terms of the Bhattacharyya coefficient $B(p, q) = \sum_x \sqrt{p(x)q(x)}$ as

$$D_{1/2}(p\|q) = -2 \log B(p, q), \quad (\text{C2})$$

and the Rényi- ∞ divergence is given by

$$D_\infty(p\|q) = \log \max_x \frac{p(x)}{q(x)}. \quad (\text{C3})$$

For the DNP transformation used in the main text, the reweighted distribution p is related to a reference distribution q via

$$p(s) = \frac{f(s) q(s)}{Z}, \quad Z = \sum_{s'} f(s') q(s'). \quad (\text{C4})$$

Substituting this relation into the definition of D_∞ gives

$$\frac{p(s)}{q(s)} = \frac{f(s)}{Z}, \quad (\text{C5})$$

so that

$$\begin{aligned} D_\infty(p\|q) &= \log \max_s \frac{p(s)}{q(s)} \\ &= \log \max_s \frac{f(s)}{Z} = \log \max_s f(s) - \log Z. \end{aligned} \quad (\text{C6})$$

Similarly,

$$\frac{q(s)}{p(s)} = \frac{Z}{f(s)}, \quad (\text{C7})$$

and therefore

$$\begin{aligned} D_\infty(q\|p) &= \log \max_s \frac{q(s)}{p(s)} \\ &= \log \max_s \frac{Z}{f(s)} = -\log \min_s f(s) + \log Z. \end{aligned} \quad (\text{C8})$$

These are the expressions used in the main text to relate the dynamic range of f to the Bhattacharyya coefficient.

Finally, we recall that Rényi divergences are monotone in the order parameter [33]: for fixed p and q , one has

$$\alpha \leq \beta \implies D_\alpha(p\|q) \leq D_\beta(p\|q), \quad (\text{C9})$$

In particular, this implies the inequality $D_{1/2}(p\|q) \leq D_\infty(p\|q)$.

We now prove Theorem 1 below. Refer to Fig. 2 in the main text.

Proof. Partition the n qubits into *kept blocks* B_1, \dots, B_m of size L , separated by *buffer regions* G of length g . Let \mathcal{B} denote the classical channel that discards the buffer sites. By monotonicity of the Rényi- $\frac{1}{2}$ divergence under stochastic maps,

$$D_{1/2}(p_n \| q_n) \geq D_{1/2}(\mathcal{B}p_n \| \mathcal{B}q_n). \quad (\text{C10})$$

Locality of finite-depth circuits. A depth- d local circuit has a light-cone radius $\ell = O(d)$. Choosing $g \gtrsim \ell$ ensures that no causal cone connects distinct kept blocks, implying that the ansatz distribution factorizes as

$$\mathcal{B}q_n = \bigotimes_{i=1}^m q_{B_i}. \quad (\text{C11})$$

Note that no assumption is made on $\mathcal{B}p_n$, which may exhibit long-range correlations. Thus, we exploit the continuity of Rényi- $\frac{1}{2}$ divergence to show that

Continuity of $D_{1/2}$. The Rényi- $\frac{1}{2}$ divergence is Lipschitz-continuous in total variation distance on compact domains [33]. Hence, there exists $C > 0$ such that for any P, Q, \tilde{Q} ,

$$|D_{1/2}(P \| \tilde{Q}) - D_{1/2}(P \| Q)| \leq C \|\tilde{Q} - Q\|_{\text{TV}}. \quad (\text{C12})$$

Applying this to $P = \mathcal{B}p_n$, $Q = \bigotimes_i q_{B_i}$, and $\tilde{Q} = \mathcal{B}q_n$ yields

$$D_{1/2}(\mathcal{B}p_n \| \mathcal{B}q_n) \geq D_{1/2}\left(\mathcal{B}p_n \middle\| \bigotimes_i q_{B_i}\right) - C\varepsilon(g), \quad (\text{C13})$$

where $\varepsilon(g) \rightarrow 0$ as the buffer length g exceeds the light-cone size.

Additivity over independent blocks. Since the product distribution $Q = \bigotimes_i q_{B_i}$ is independent across blocks, the Rényi- $\frac{1}{2}$ divergence is additive:

$$D_{1/2}\left(\mathcal{B}p_n \middle\| \bigotimes_i q_{B_i}\right) = \sum_{i=1}^m D_{1/2}(p_{B_i} \| q_{B_i}). \quad (\text{C14})$$

By assumption of a nonzero local gap $\delta^* > 0$, each block satisfies $D_{1/2}(p_{B_i} \| q_{B_i}) \geq \delta^*$.

Substituting Eqs. (C10)–(C14) and choosing g such that $C\varepsilon(g) \leq \delta^*/2$ gives

$$D_{1/2}(p_n \| q_n(\theta_{\text{tr}})) \geq m \frac{\delta^*}{2}, \quad m \simeq \frac{n}{L}. \quad (\text{C15})$$

Hence,

$$D_{1/2}(p_n \| q_n(\theta_{\text{tr}})) \geq \frac{\delta^*}{2L} n.$$

Recalling that $B(p, q) = \exp[-D_{1/2}(p \| q)/2]$, we obtain

$$B(p_n, q_n(\theta_{\text{tr}})) \leq \exp\left(-\frac{\delta^*}{4L} n\right). \quad (\text{C16})$$

Appendix D: Proof of exponential decay of Bhattacharyya coefficient: linear-depth circuit

Here, we prove that for random unitary 2-design circuits, the Bhattacharyya coefficient decays exponentially to the number of qubits 2.

Proof. Under the Haar measure on the complex unit sphere $\mathbb{S}^{2d-1} \subset \mathbb{C}^d$, the joint distribution of probabilities $\mathbf{q} = (q(1), \dots, q(d))$ follows the symmetric Dirichlet law $\text{Dirichlet}(\alpha_1 = \dots = \alpha_d = 1)$ [34, 35]. The marginal distribution of each component is therefore

$$q \sim \text{Beta}(\alpha = 1, \beta = d-1), \quad f(q) = (d-1)(1-q)^{d-2}, \quad (\text{D1})$$

as given in Ref. [36, Sec. 49]. Using the standard Beta-moment identity,

$$\mathbb{E}[q^k] = \frac{B(\alpha+k, \beta)}{B(\alpha, \beta)} = \frac{\Gamma(\alpha+k)\Gamma(\alpha+\beta)}{\Gamma(\alpha)\Gamma(\alpha+\beta+k)}, \quad (\text{D2})$$

and substituting $\alpha = 1, \beta = d-1$, one obtains

$$\mathbb{E}[q^k] = \frac{\Gamma(1+k)\Gamma(d)}{\Gamma(d+k)}. \quad (\text{D3})$$

In particular, for the Haar amplitude magnitude \sqrt{q} ,

$$\mathbb{E}_{\text{Haar}}[\sqrt{q}] = \frac{\Gamma(3/2)\Gamma(d)}{\Gamma(d+1/2)} \simeq \frac{\sqrt{\pi}}{2} d^{-1/2}, \quad (\text{D4})$$

where the asymptotic form follows from $\Gamma(d)/\Gamma(d+1/2) = d^{-1/2}(1+O(d^{-1}))$.

Therefore, each computational-basis amplitude of a Haar-random quantum state has an expected magnitude of order $O(d^{-1/2})$. For an n -qubit system ($d = 2^n$), the Bhattacharyya coefficient between a fixed distribution $p(s)$ and the Haar-distributed measurement distribution $q(s)$ is given by

$$\begin{aligned} \mathbb{E}_{\text{Haar}}[B(p, q)] &= \sum_s \sqrt{p(s)} \mathbb{E}_{\text{Haar}}[\sqrt{q(s)}] \\ &= \Theta(2^{-n/2}) \sum_s \sqrt{p(s)}. \end{aligned} \quad (\text{D5})$$

The exponential suppression $2^{-n/2}$ originates universally from Haar randomness, while the prefactor $\sum_s \sqrt{p(s)}$ depends only on the structure of the fixed distribution $p(s)$.

To bound fluctuations, we invoke the following form of Lévy's lemma [35]:

Lemma 1 (Lévy's lemma). *For an L -Lipschitz function $f : \mathbb{S}^{d-1} \rightarrow \mathbb{R}$ on the $(d-1)$ -sphere,*

$$\Pr(|f(\psi) - \mathbb{E}f| \geq t) \leq 2 \exp[-cdt^2/L^2], \quad (\text{D6})$$

for a universal constant $c > 0$. \square

Applying this to $f(|\psi\rangle) = \sum_s \sqrt{p(s)} |\langle s|\psi\rangle|$ shows that $B(p, q)$ is exponentially concentrated around its mean with variance scale $O(2^{-n})$, yielding

$$B(p, q) = \Theta(2^{-n/2}) \quad \text{with probability } 1 - e^{-\Omega(2^n)}.$$

□

Combining with the general bound $r \geq B(p, q)^{-4}$ [Eq. (21)] gives the exponential scaling of Eq. (24). Thus, when a circuit forms a unitary 2-design, the overlap between the state represented by the circuit and the ground state is exponentially small.

Appendix E: Possibilities of measurement-derived divergence for VQE variants with non-unitary transformations.

DNP is not the only way to utilize non-unitary transformation onto VQE. Several research efforts attempt to apply additional gates and post-processing in a non-unitary fashion in order to achieve better performance in terms of accuracy, especially for the eigensolvers with hardware-efficient ansätze. We briefly review potentials for measurement-derived divergence discussed in our work for several studies that utilize non-unitary transformations onto the states and discuss their resource efficiencies compared to our work.

One such research is called the non-unitary variational quantum eigensolver (nu-VQE) [37]. It performs non-unitary operation as a set of quantum gates applied on top of the prepared ansatz. In specific, the work makes use of the single-body and two-body Jastrow factors [38] as its non-unitary process. The Jastrow operator takes the form

$$J = J_1 + J_2, \\ J_1 = \exp \left[- \sum_{i=1}^N \alpha_i Z_i \right], J_2 = \exp \left[- \sum_{i < j}^N \lambda_{i,j} Z_i Z_j \right], \quad (\text{E1})$$

where α_i and $\lambda_{i,j}$ are trainable parameters, equivalent to the parameters of the neural network in the case of VQNHE. The overall Jastrow operator is approximated to its linear form for simplicity

$$J(\vec{\alpha}, \vec{\lambda}) = 1 - \sum_{i=1}^N \alpha_i Z_i - \sum_{i < j}^N \lambda_{i,j} Z_i Z_j. \quad (\text{E2})$$

As acting $J(\vec{\alpha}, \vec{\lambda})$ is non-unitary, similar to VQNHE, nu-VQE requires normalization to obtain the energy. Let $|\psi\rangle := |\psi(\vec{\theta})\rangle$ and $J := J(\vec{\alpha}, \vec{\lambda})$, and define $\langle A \rangle :=$

$\langle \psi | A | \psi \rangle$. The energy then reads

$$E = \frac{\langle J^\dagger H J \rangle}{\langle J^\dagger J \rangle} \\ = \frac{\sum_P c_P \left(\langle P \rangle - \sum_i \alpha_i \langle P Z_i \rangle - \sum_{i < j} \lambda_{i,j} \langle P Z_i Z_j \rangle \right)}{1 - \sum_i \alpha_i \langle Z_i \rangle - \sum_{i < j} \lambda_{i,j} \langle Z_i Z_j \rangle}. \quad (\text{E3})$$

The equation on the second line of Eq. (E3) is obtained by writing down the Jastrow factor (Eq. (E2)) explicitly in its linear form.

Going through the scenarios of divergence in the paper, the first obvious possibility is that viewing the parameters $\vec{\alpha}, \vec{\lambda}$ as variables, any coefficient on the denominator yields zero and the corresponding one on the numerator gives nonzero value. This corresponds to the case where bit strings out of measurement process are missing on the denominator side, causing severe failure of the algorithm. Nevertheless, this is not a realistic situation in terms of nu-VQE. In order to satisfy the conditions, it must be the case where $\exists i$ such that $\langle \psi | \hat{Z}_i | \psi \rangle = 0, \langle \psi | \hat{P} \hat{Z}_i | \psi \rangle \neq 0$ or $\exists i, j$ such that $\langle \psi | \hat{Z}_i \hat{Z}_j | \psi \rangle = 0, \langle \psi | \hat{P} \hat{Z}_i \hat{Z}_j | \psi \rangle \neq 0$. Although not theoretically impossible, getting an exact zero as an expectation value is highly unlikely, unless one happens to prepare an exactly balanced state as $|\psi\rangle$ or the number of measurement outcomes yielding -1 for Z_i equals the number yielding $+1$. In such rare cases, it might experience similar failure to VQNHE, although this is not considered a major flaw of the algorithm.

Despite its idea of applying a non-unitary transformation without significant risk of divergence and thus without concerns of scalability bottleneck due to number of shots, nu-VQE requires many more quantum circuit evaluations than VQNHE or U-VQNHE. As written in Eq. (E2), in order to provide the expectation values to all the terms, it requires at most $O(n^4)$ quantum circuit evaluations for each Pauli term comprising the target Hamiltonian. Note that this is minimal overhead of using the Jastrow factor at its linear approximation. Any higher-ordered terms require much more circuits, and the exact Jastrow factor demands exponential of them. Thus, VQNHE and U-VQNHE require much less computational resources in terms of the quantum computations, while requiring only polynomially scaling classical resources.

Another attempt to apply non-unitary transformation, named Jastrow quantum circuit (JQC) [39], applies the transformation variationally on the ansatz state itself while mapping operators to the qubit space via, for example, Jordan-Wigner transformation [40]. The projector that implements Jastrow operator is written as

$$\mathcal{P}_J = e^J, J = \sum_{k \neq l} \lambda_{kl} Z_k Z_l. \quad (\text{E4})$$

Note that it captures the second-order terms of Eq. (E1) while not exploiting its linear approximation form. In

Ref. [39] it is argued that the nonunitary Jastrow operator effectively filters out components that yield high energy eigenvalues.

Although the detailed implementation and approximation details differ, JQC and nu-VQE actually end up with the same procedure from the expectation value point-of-view. The difference comes from the target on which the Jastrow operator acts. Thus, in terms of possible divergence, the same arguments on nu-VQE apply for non-unitary transformations by projective mapping of states. In addition, in terms of resource efficiency, it experiences the same overhead in the number of quantum circuits required, making VQNHE and U-VQNHE superior considering the resource overhead.

Alternatively, there exists a variant of VQE that exploits non-unitary transformation in a different fashion. Cascaded variational quantum eigensolver (CVQE) [41] constructs its ansatz in the Fock space, which is mapped to the qubit space similar to the JQC, and applies the following additional non-unitary transformation in the occupation number eigenstates

$$\hat{\lambda}(\phi) = \sum_{n \in \mathcal{N}} \lambda_n(\phi) |n\rangle \langle n|, \quad (\text{E5})$$

which lets the transformed state to be written as

$$|\psi(\phi)\rangle = e^{i\hat{\lambda}(\phi)} \hat{U} |0\rangle = e^{i\hat{\lambda}(\phi)} |\psi_0\rangle, \quad (\text{E6})$$

where U is a unitary operator and $|0\rangle$ represents the vacuum state, written in the second quantization picture. It can be a fixed operator or be trained with simple ansätze, just as hardware-efficient ansatz block is trained in VQNHE before optimizing parameters of the neural network. The result of the expectation value of the given Hamiltonian can then be written as

$$E = \frac{\langle \psi_0 | e^{i\hat{\lambda}^\dagger(\phi)} \hat{H} e^{i\hat{\lambda}(\phi)} | \psi_0 \rangle}{\langle \psi_0 | e^{i\hat{\lambda}^\dagger(\phi)} e^{i\hat{\lambda}(\phi)} | \psi_0 \rangle}. \quad (\text{E7})$$

The key difference between the previous algorithms and CVQE is that each variational parameter $\lambda_n(\phi)$ is associated with a number state, or a Fock state $|n\rangle$, whereas for the previous algorithms the parameters were associated with the Jastrow terms. As there are exponentially many terms comprising $e^{i\hat{\lambda}^\dagger(\phi)} \hat{H} e^{i\hat{\lambda}(\phi)}$, CVQE expresses the expectation values as that linear combination of operators $\{\hat{R}_{lm}\}$, which can be obtained analytically, that express the expectation value in a diagonal form. Note that the scheme is similar to DNP, except that one does not explicitly utilize neural network for post-processing. Due to the direct dependence of the parameters, the gradient of the energy with respect to the parameters ϕ can be analytically obtained. Note that the given transformation on the ansatz state resembles that of U-VQNHE, except that U-VQNHE restricts the values of λ_n to real numbers.

So is CVQE vulnerable to instabilities during optimization? The expectation value, written in terms of the set

of operators $\{\hat{R}_{lm}^\dagger\}$, is

$$\begin{aligned} \Gamma(\phi) &= \sum_{l,m,n} v_{lmn} e^{-i\lambda_{n_l^+}^*(\phi)} e^{i\lambda_{n_l^-}(\phi)} |\langle \psi_0 | \hat{R}_{lm}^\dagger | n \rangle|^2 \\ \Lambda(\phi) &= \sum_n e^{-2\text{Im}\lambda_n(\phi)} |\langle \psi_0 | n \rangle|^2 \\ E &= \frac{\Gamma(\phi)}{\Lambda(\phi)}, \end{aligned} \quad (\text{E8})$$

where \mathcal{L} represents indices of the terms in Hamiltonian expressed as $\hat{H} = \sum_{l \in \mathcal{L}} h_l C_{n_l^+}^\dagger C_{n_l^-}$, \mathcal{M}_l represents the basis of the Hilbert space spanned by the supports of each term $C_{n_l^+}^\dagger C_{n_l^-}$, and v_{lmn} is a coefficient depending on these indices. Note, similar to how DNP is implemented on a shot-basis, that $|\langle \psi_0 | \hat{R}_{lm}^\dagger | n \rangle|^2$ and $|\langle \psi_0 | n \rangle|^2$ are the counts of each bit strings (Jordan-Wigner transformation [40] maps each number state $|n\rangle$ into qubit state $\bigotimes_{q \in \mathcal{Q}} |n_q\rangle \in \mathcal{H}_Q$). In addition, each $\lambda_n(\phi)$ is multiplied by $|\langle \psi_0 | \hat{R}_{lm}^\dagger | n \rangle|^2$ on the numerator and $|\langle \psi_0 | n \rangle|^2$ on the denominator. Thus, it follows that CVQE is likely to diverge or yield inaccurate values, unless it is given with an exponential scale of shots.

Analogous to our work, in order to maintain the structure of CVQE while preventing aforementioned divergence under reasonable amount of shots, it must be guaranteed that $\forall n, \lambda_n(\phi) \in \mathbb{R}$, which resembles the unitary transformation from the neural network of the main text. By confining the parametrized operator $\hat{\lambda}(\phi)$ thus to be unitary, CVQE loses its ability to seek beyond the Fock space as asserted by its authors, although the actual solution lives in the Fock space. However, combining how CVQE handles diagonalization of the terms comprising the Hamiltonian described in the Fock space onto the framework of U-VQNHE presents potentials for a resource-efficient variational algorithm applicable in the second quantization formalism. The lack of expressiveness of the postprocessing alone can be leveraged by utilizing a hardware-efficient VQE as a unitary operator acting on the vacuum state and train both parameters in sequence. In addition, with use of hardware-efficient ansatz for the initial unitary, the post-processing can adopt neural network for generality and expressiveness.

In short, there are several other variants of VQE that utilizes non-unitary transformation to enhance the expressiveness. While algorithms that makes use of Jastrow factor to modify the quantum state mapping [39] or the Hamiltonian [37] are unlikely to experience the divergence during the optimization of the parameters of the non-unitary transformations, they require much more quantum resources than VQNHE or U-VQNHE and thus are not as resource-efficient. On the other hand, CVQE [41] displays resemblance to VQNHE in terms of how they evaluate the expectation value with respect to the parameters, and our analysis indicates that CVQE also requires an exponential amount of measurements to

be taken to evaluate the denominator to prevent itself from divergence issues. Thus, no algorithm among those listed above presents better resource-efficiency than U-VQNHE considering both the number of quantum circuits to be evaluated and the number of shots to be taken.

Appendix F: Notes on the neural network

For studies that involve training of neural networks, setting the hyperparameters related to its training is of significant importance. However, in terms of the neural network used in this research, which consists of two fully-connected layers and a series of activation functions, including ReLU, sigmoid and tanh functions, training of it is not as difficult of a work compared to state-of-the-art neural network researches. Nevertheless, there are several aspects of it worth mentioning.

The DNP and U-VQNHE system consist of two sets of parameters: variational parameters for the quantum circuits and the parameters for the classical neural network. All simulations in the research have been conducted by training the VQE first, and then training the neural network on top of the already trained VQE. The reason for that is that, possible as it may seem, joint

training of the parameters is impossible in the case of DNP. When the VQE output is fixed, the neural network evaluation is deterministic, and its optimization is stable, whereas when the output of the quantum circuit is not fixed, it yields deviations on every measurement process. For joint training, this is a critical limitation, as the VQE yields unstable outputs and the neural network struggles to find a way to be trained such that it consistently provides downward gradient. Moreover, repetitive evaluation of the quantum circuit is very costly, making joint training very inefficient.

In terms of optimization tools, gradient-free COBYLA optimizer [42] has been used for optimizing the parameters of VQE and ADAM for the neural network. Nevertheless, one can also choose to use parameter-shift rule [43] to obtain the quantum gradients of the given ansatz circuit and use gradient-based optimization techniques, such as stochastic gradient-descent optimization. In order to apply the parameter-shift rule, all the parametrized gates must have their generators with two unique eigenvalues. As our choice of hardware-efficient ansatz consists only of RX and RZZ gates as parametrized gates, they all fall under the criterion, allowing for easy usage of the parameter-shift rule.

[1] A. Peruzzo, J. McClean, P. Shadbolt, M.-H. Yung, X.-Q. Zhou, P. J. Love, A. Aspuru-Guzik, and J. L. O’Brien, A variational eigenvalue solver on a photonic quantum processor, *Nature Communications* **5**, 4213 (2014).

[2] J. Tilly, H. Chen, S. Cao, D. Picozzi, K. Setia, Y. Li, E. Grant, L. Wossnig, I. Rungger, G. H. Booth, and T. O’Brien, The variational quantum eigensolver: A review of methods and best practices, *Phys. Rep.* **986**, 1 (2022).

[3] S. McArdle, S. Endo, A. Aspuru-Guzik, S. C. Benjamin, and X. Yuan, Quantum computational chemistry, *Rev. Mod. Phys.* **92**, 015003 (2020).

[4] H. Lim, D. H. Kang, J. Kim, A. Pellow-Jarman, S. McFarthing, R. Pellow-Jarman, H.-N. Jeon, B. Oh, J.-K. K. Rhee, and K. T. No, Fragment molecular orbital-based variational quantum eigensolver for quantum chemistry in the age of quantum computing, *Sci. Rep.* **14**, 2422 (2024).

[5] A. A. Balushki, J. L. Romero, and M. Saffman, Real-time hamiltonian estimation using continuous quantum measurement, *Phys. Rev. Applied* **21**, 064017 (2024).

[6] J. Preskill, Quantum computing in the NISQ era and beyond, *Quantum* **2**, 79 (2018).

[7] J. Macdonald, Successive approximations by the rayleigh-ritz variation method, *Physical Reviews* **43**, 830 (1933).

[8] M. Cerezo, A. Arrasmith, R. Babbush, S. C. Benjamin, S. Endo, K. Fujii, J. R. McClean, K. Mitarai, X. Yuan, L. Cincio, and P. J. Coles, Variational quantum algorithms, *Nature Reviews Physics* **3**, 625 (2021).

[9] E. Farhi, J. Goldstone, and S. Gutmann, A quantum approximate optimization algorithm (2014), [arXiv:1411.4028 \[quant-ph\]](https://arxiv.org/abs/1411.4028).

[10] P.-L. Dallaire-Demers and N. Killoran, Quantum generative adversarial networks, *Physical Review A* **98**, 012324 (2018).

[11] S. Lloyd and C. Weedbrook, Quantum generative adversarial learning, *Physical Review Letters* **121**, 040502 (2018).

[12] I. Cong, S. Choi, and M. D. Lukin, Quantum convolutional neural networks, *Nature Physics* **15**, 1273 (2019).

[13] J. Bausch, Recurrent quantum neural networks, in *Advances in Neural Information Processing Systems 33 (NeurIPS 2020)* (2020).

[14] A. Pérez-Salinas, A. Cervera-Lierta, E. Gil-Fuster, and J. I. Latorre, Data re-uploading for a universal quantum classifier, *Quantum* **4**, 226 (2020).

[15] M. Schuld and N. Killoran, Quantum machine learning in feature hilbert spaces, *Physical Review Letters* **122**, 040504 (2019).

[16] E. Grant, L. Wossnig, M. Ostaszewski, and M. Benedetti, An initialization strategy for addressing barren plateaus in parametrized quantum circuits, *Quantum* **3**, 214 (2019).

[17] A. Mari, T. R. Bromley, J. Izaac, M. Schuld, and N. Killoran, Transfer learning in hybrid classical-quantum neural networks, *Quantum* **4**, 340 (2020).

[18] J. Miao, C.-Y. Hsieh, and S.-X. Zhang, Neural network encoded variational quantum algorithms (2023), [arXiv:2308.01068 \[quant-ph\]](https://arxiv.org/abs/2308.01068).

[19] S. Bravyi, S. Sheldon, A. Kandala, D. C. Mckay, and J. M. Gambetta, Mitigating measurement errors in multiqubit experiments, *Physical Review A* **103**, 042605 (2021).

[20] P. D. Nation, H. Kang, H. P. Liu, N. M. Sundaresan, and J. M. Gambetta, Scalable mitigation of measurement errors on quantum computers, *PRX Quantum* **2**, 040326 (2021).

[21] A. Lowe, T. Giurgica-Tiron, D. Stilck Fran  a, A. Green, and N. Killoran, Unified approach to data-driven quantum error mitigation, *Physical Review Research* **3**, 033098 (2021).

[22] D. Wecker, M. B. Hastings, and M. Troyer, Progress towards practical quantum variational algorithms, *Physical Review A* **92**, 042303 (2015), measurement strategies and grouping of Pauli terms via basis changes.

[23] S.-X. Zhang, Z.-Q. Wan, C.-K. Lee, C.-Y. Hsieh, S. Zhang, and H. Yao, Variational quantum-neural hybrid eigensolver, *Physical Review Letters* **128**, 120502 (2022).

[24] P. Neal, The generalized coupon-collector problem, *J. Appl. Probab.* **45**, 621 (2008).

[25] M. Ren, Y.-C. Chen, Y. Ye, M.-H. Hsieh, A. Hu, and C.-Y. Hsieh, A neural-guided variational quantum algorithm for efficient sign structure learning in hybrid architectures (2025), [arXiv:2507.07555 \[quant-ph\]](https://arxiv.org/abs/2507.07555).

[26] J. R. McClean, S. Boixo, V. N. Smelyanskiy, R. Babbush, and H. Neven, Barren plateaus in quantum neural network training landscapes, *Nature Communications* **9**, 4812 (2018).

[27] M. Cerezo, A. Sone, T. Volkoff, L. Cincio, and P. J. Coles, Cost function dependent barren plateaus in shallow parametrized quantum circuits, *Nature Communications* **12**, 1791 (2021).

[28] A. W. Harrow and R. A. Low, Random quantum circuits are approximate 2-designs, *Communications in Mathematical Physics* **291**, 257–302 (2009).

[29] S.-X. Zhang, J. Miao, and C.-Y. Hsieh, Variational post-selection for ground-state and thermal-state simulation, *Quantum Sci. Technol.* **10**, 015028 (2025).

[30] W. Li, S.-X. Zhang, Z. Sheng, C. Gong, and Z. Shuai, Quantum machine learning of molecular energies with hybrid quantum–neural wavefunction approach, *RSC Advances* **15**, 6424 (2025).

[31] T. M. Henderson, I. W. Bulik, and G. E. Scuseria, Pair extended coupled cluster doubles, *The Journal of Chemical Physics* **142**, 214116 (2015).

[32] S.-X. Zhang, J. Miao, C.-K. Lee, H. Yao, and C.-Y. Hsieh, Variational quantum-neural hybrid error mitigation, *Adv. Quantum Technol.* **6**, 2300147 (2023).

[33] T. van Erven and P. Harremo  s, R  nyi divergence and Kullback–Leibler divergence, *IEEE Transactions on Information Theory* **60**, 3797 (2014).

[34] K.   yczkowski and H.-J. Sommers, Induced measures in the space of mixed quantum states, *J. Phys. A: Math. Gen.* **34**, 7111 (2001).

[35] M. Ledoux, *The Concentration of Measure Phenomenon*, Mathematical Surveys and Monographs, Vol. 89 (American Mathematical Society, Providence, RI, 2001).

[36] N. L. Johnson, S. Kotz, and N. Balakrishnan, *Continuous Multivariate Distributions, Volume 1: Models and Applications*, 2nd ed. (Wiley, 2000).

[37] F. Benfenati, G. Mazzola, C. Capecci, P. K. Barkoutsos, P. J. Ollitrault, I. Tavernelli, and L. Guidoni, Improved accuracy on noisy devices by nonunitary variational quantum eigensolver for chemistry applications, *J. Chem. Theory Comput.* **17**, 3946 (2021).

[38] R. Jastrow, Many-body problem with strong forces, *Phys. Rev.* **98**, 1479 (1955).

[39] G. Mazzola, P. J. Ollitrault, P. K. Barkoutsos, and I. Tavernelli, Nonunitary operations for ground-state calculations in near-term quantum computers, *Phys. Rev. Lett.* **123**, 130501 (2019).

[40] J.-M. Reiner, M. Marthaler, J. Braum  ller, M. Weides, and G. Sch  n, Emulating the one-dimensional fermi–hubbard model by a double chain of qubits, *Phys. Rev. A* **94**, 032338 (2016).

[41] D. Gunlycke, C. S. Hellberg, and J. P. T. Stenger, Cascaded variational quantum eigensolver algorithm, *Phys. Rev. Res.* **6**, 013238 (2024).

[42] M. J. D. Powell, *A direct-search optimization method that models the objective and constraint functions by linear interpolation*, Tech. Rep. NA1994/05 (University of Cambridge, DAMTP, 1994).

[43] D. Wierichs, J. Izaac, C. Wang, and C. Y. Lin, General parameter-shift rules for quantum gradients, *Quantum* **6**, 677 (2022).